

**STRESS MODELLING OF WELDED TITANIUM ALLOY  
(GRADE 5) PIPES**

**Etienyng Edem Inyang  
206070365**

**A thesis submitted in fulfillment of the requirements for the degree of  
Magister Technologiae: Engineering: Industrial**

**Department: Industrial Engineering and Operations Management  
Faculty of Engineering and Technology  
Vaal University of Technology  
Vanderbijlpark**

**Supervisor:  
Prof P. Mendonidis**

**Co-supervisors:  
Dr P. Oba and Prof L. M. Masu**

**December 2010**

## **DECLARATION**

I declare that this dissertation is my own work. It is submitted for the degree of Magister Technologiae: Engineering: Industrial, to the Department of Industrial Engineering and Operations Management at the Vaal University of Technology, Vanderbijlpark. It has not been submitted before for any degree and is not being concurrently submitted in candidature for any degree.

Signed .....

Date .....

## **ACKNOWLEDGEMENTS**

I wish to express my appreciation to the following:

- Professor P. Mendonidis, Dr P. Oba and Professor L. M. Masu, for their supervision and guidance during the period of this research.
- My Head of Department, Dr H. M. Campbell, who approved the acquisition of the analysis software soon after assuming office.
- My brother, Rev. Dr Iffiock Edem Inyang, MSP, for his love, encouragement and financial support during the period of this research.
- The other members of my family, for their love and prayers.
- Mr Olivier Mvudi, for his technical assistance and noteworthy answers to my numerous questions.
- Mr Andrew Analo, for his encouragement and assistance.
- The Pyrates Confraternity, especially its members ‘on board’ *Okavango*; for their fraternal encouragement.
- Almighty God, for His love and mercies throughout the duration of this research work.

## **DEDICATION**

To my mother, Gertrude Adiah Inyang  
and my late father, Anselm Robert Inyang

## **ABSTRACT**

This research work focused on welded titanium alloy (grade 5) pipes, to ascertain if the weld joints can withstand the immediate and accumulated effects of fluid flow in (industrial) applications.

Modeling of welded pipes was done using Pro/ENGINEER Wildfire 5.0. The cylindrical pipe models were of 206,375mm inner and 219,075mm outer diameter respectively; made of Ti6Al4V material. Three models were made: one of unwelded pipes, another with a seam weldment and the third with a circumferential weld. The welds were modeled as autogenous gas tungsten arc welding and the models included calculated heat affected zones. The pipes were modeled with a flowing fluid under pressure exerted evenly on all sides of the pipe walls (circumference). The boundary conditions were such that the pipe ends were supported as if the pipe were continuous.

Stress and strain analysis on the pipe models were performed by the Finite Element Method using Pro/ENGINEER Wildfire 5.0. The results of the Finite Element Analysis (FEA) indicated that stress vary very negligibly along the pipe. A comparison of the FEA modeling results to the analytically determined value of the stress showed very low or zero percentage deviation.

## TABLE OF CONTENT

<b>Declaration</b>	<b>ii</b>
<b>Acknowledgement</b>	<b>iii</b>
<b>Dedication</b>	<b>iv</b>
<b>Abstract</b>	<b>v</b>
<b>Table of content</b>	<b>vi</b>
<b>List of figures</b>	<b>ix</b>
<b>List of tables</b>	<b>x</b>
<b>List of appendices</b>	<b>xi</b>
<b>Chapter 1    Introduction</b>	<b>1</b>
1.1        Background	1
1.1.1    Weld Metal Porosity	3
1.1.2    Embrittlement	4
1.1.3    Contamination cracking	4
1.2        Welding	5
1.3        Problem Statement	6
1.4        Specific Objectives of the Research	6
1.5        Value of the Research	7
1.6        Research Methodology	8
<b>Chapter 2    Review of FEA, pipes, welding, titanium, Ti4Al6V, and the joining of titanium</b>	<b>10</b>
2.1        Introduction	10
2.2        Finite Element Analysis (FEA)	10
2.3        Pipes	12
2.4        Welding	13

2.4.1	Welding processes	15
2.4.1.1	Gas-tungsten arc welding (GTAW)	16
2.4.1.2	Gas-metal arc welding (GMAW)	18
2.4.1.3	Plasma arc welding (PAW)	18
2.4.1.4	Electron-beam welding (EBW)	19
2.4.1.5	Laser-beam welding (LBW)	20
2.4.1.6	Friction welding (FW)	21
2.4.1.6.1	Linear Friction Welding (LFW)	23
2.4.1.6.2	Friction Stir Welding (FSW)	24
2.4.1.7	Resistance welding (RW)	25
2.5	Filler material and electrodes	26
2.5.1	Filler-metals	26
2.5.2	Shielding gases	26
2.5.3	Electrodes	27
2.6	Titanium	28
2.7	Ti6Al4V	29
2.8	Titanium welding	30
2.9	The heat affected zone	31
2.10	Factors considered in the welding of titanium	36
<b>Chapter 3</b>	<b>Pipe Modelling and Simulation</b>	<b>41</b>
3.1	Introduction	41
3.2	Properties of materials of the Models	42
3.3	Dimensions of the Pipes	45
3.4	Pipe modelling	46
<b>Chapter 4</b>	<b>Finite Element Analysis Results and Discussion</b>	<b>57</b>
4.1	Introduction	57
4.2	FEM Results	57

4.3	Discussion of FEM Results	64
4.3.1	The Unwelded (control) Pipe Models	66
4.3.2	The “Circumference Weld” Pipe Model (CW)	68
4.3.3	The “Seam Weld” Pipe Model (SWP)	69
4.3.4	Discussion	70
<b>Chapter 5 Conclusion</b>		<b>72</b>
<b>REFERENCES</b>		<b>73</b>
<b>Appendices</b>		<b>82</b>

## List of figures

Fig 2.1	Principle of friction welding process. (A) Store kinetic energy in flywheel and apply controlled end force. (B) Rotation ceases and weld is complete.	23
Fig 2.2	The Titanium Aluminium Phase Diagram (expressed in atomic percent).	31
Fig 2.3	The Titanium Aluminium Phase Diagram (expressed in weight percent).	32
Fig 2.4	The Titanium Vanadium Phase Diagram.	34
Fig 2.5	Pseudo-binary phase diagram of Ti6Al4V.	35
Fig 3.1	Unwelded pipe (Control) model of 1000 mm length showing constraints, flow, and pressure.	47
Fig 3.2	Unwelded pipe (Control) model of 50 mm length showing constraints, flow, and pressure.	48
Fig 3.3	“Seam-weld” pipe (SWP) model of 1000 mm length showing constraints, flow, and pressure.	49
Fig 3.4	“Seam-weld” pipe (SWP) model of 50 mm length showing constraints, flow, and pressure.	50
Fig 3.5	“Circumference weld” (CW) pipe model of 1000 mm length showing constraints, flow, and pressure.	51
Fig 3.6	“Circumference weld” (CW) pipe model of 50 mm length showing constraints, flow, and pressure.	52
Fig 4.1a	Stress distribution along the 1000 mm (unwelded) pipe model.	58
Fig 4.1b	Stress distribution along the 50 mm (unwelded) pipe model.	59
Fig 4.2a	Stress distribution along the 1000 mm “circumference weld” (CW) pipe model.	60
Fig 4.2b	Stress distribution along the 50 mm “circumference weld” (CW) pipe model.	61
Fig 4.3a	Stress distribution along the 1000 mm “seam weld” pipe model.	62
Fig 4.3b	Stress distribution along the 50 mm “seam weld” pipe model.	63

## List of tables

Table 1.1	Common ASTM Titanium alloy grades and their weldability.	2
Table 1.2	Weldability of selected non-ASTM Titanium alloys.	3
Table 2.1	Bend Strength of Materials and Welds.	17
Table 2.2	Types of weld Weld.	17
Table 2.3	Impurity content (wt%) of CP-Ti filler materials.	17
Table 2.4	Tensile properties of selected welds in 6.35mm thickness of Ti-6Al-4V.	25
Table 2.5	Tungsten alloys, for use in GTAW electrodes.	27
Table 2.6	Comparison of Welding processes based on Cost.	36
Table 2.7	Nominal Chemical composition of common commercial titanium alloy grades.	37
Table 2.8	Titanium welded joint design.	38
Table 2.9	Titanium welding electrode composition (AWS A5.16-70).	39
Table 2.10	Comparison of Welding processes based on the Ease with which they can be performed.	40
Table 3.1	Tensile Properties for TIMETAL 6-4.	43
Table 3.2	Physical Properties for TIMETAL 6-4.	44
Table 3.3	ANSI pipe schedules, indicating wall thickness (in inches).	45
Table 3.4	Dimensions of models (and their component parts).	53
Table 4.1	FEM Results.	57
Table 4.2	Percentage deviation of simulated von Mises stress results from the calculated hoop stress value	66

## **List of appendices**

Appendix A	Simulation result Summary for Structural (static) Design Study of 1000 mm “unwelded” pipe model.	82
Appendix B	Simulation result Log for Structural (fatigue) Design Study of 1000 mm “circumference weld” pipe model.	88
Appendix C	Simulation result Summary for Structural (static) Design Study of 1000 mm “seam weld” pipe model	91
Appendix D	Simulation result Log for Structural (fatigue) Design Study of 50 mm “unwelded” pipe model	97

# **Chapter 1 Introduction**

## **1.1 Background**

Titanium is a unique material because it has very good physical properties – high strength, low density, good ductility, and a relatively high melting point. It is as strong as some alloys of steel, but about 45% lighter than those steel alloys (Barksdale & Jelks, 1968: 738). In all fields of engineering, design, and fabrication, titanium and its alloys are considered for use, in a continuously widening range of applications. Presently, cost, availability, and fabrication difficulties limit the use of titanium despite all the excellent benefits which titanium and its alloys offer. The variety of titanium alloys, and the even greater variety of engineering metals and materials, require that there should be a versatile selection of joining processes for titanium, if the metal is to be of common use in the widest possible range of applications. And titanium (grade 5) alloy is the most commonly used alloy of the metal industrially ([www.timet.com](http://www.timet.com)). Among other industries, it is applied in the petrochemical sector and in aerospace technology, and can be used primarily in the oil and gas sector as well. Although mechanical fastening, adhesion, and other techniques have their place; welding continues to be the most important process for joining titanium. According to Cary and Helzer (2005: 45-49), welding of titanium by various processes is widely practiced, and service performance of welds is proven with an extensive and continuously extending record of achievements. Newer methods adaptable for titanium are further advancing the science, technology, and economics of welding.

In comparison with other metals, the most useful properties of titanium are its resistance to corrosion, and the fact that it has the highest strength-to-weight ratio of any metal (Donachie, 2000: 11). The mechanical properties of titanium constitute very important criteria considered by design engineers in production processes. Titanium alloys joined by any one of the wide range of welding processes are routinely at work in applications such as aircraft (high strength, in combination with low density), aero engines (high strength, low density and good creep resistance of up to about 550°C), pressure vessels/offshore platform pipe networks (corrosion resistance, high strength, low

density), biomedical services/implants for the human body (corrosion resistance and high strength), components in chemical processing equipment (corrosion resistance), and even ultra lightweight roofing (Lutjering & Williams, 2003: 1-3). For these and more applications, it is critical for the design engineer to consider the variation in the mechanical behaviour of the different alloy grades when making the material selection. Practical and comparative welding processes may ensure that there are few other materials that can compete technically or economically with the performance provided by titanium (Cary & Helzer, 2005: 42-62).

Alloys, including titanium alloys, can be joined by solid state welding processes. They can also be joined by fusion welding, which involves the use of heat, and sometimes a filler material such as a consumable electrode. The weldability of titanium alloys is usually assessed on the basis of the toughness and ductility of the weld metal. Commercially pure grades are considered very easy to fabricate and are ordinarily used in the as-welded condition. Titanium alloys show reduced weld metal ductility and toughness. Tables 1.1 and 1.2 show the weldability of the common titanium grades and other alloys listed by the American Society for Testing and Material Standards (ASTM).

**Table 1.1: Common ASTM Titanium alloy grades and their weldability.**

ALLOY GRADE	WELDABILITY	COMMENTS
1, 2, 3, 4, 7, 11, 12, 13, 14, 15, 16, 17, 26, 27	Excellent	Commercially pure and low alloy grades with minor additions of Pd, Ru, Mo etc.
9, 18, 28	Excellent	Ti-3Al-2.5V grades.
5, 23, 24, 29	Fair-good	Ti-6Al-4V grades.
21	Excellent	Beta alloys
6, 6ELI	Good-Excellent	Ti-5Al-2.5Sn

Hass (2006: 9-10) observed that welds in titanium are substantially immuned to many of the weld cracking problems common in ferrous alloy fabrications. Yet, despite this and other beneficial characteristics, some engineers still believe that titanium is difficult to weld; possibly due to its particular requirements with regards to gas shielding, or that it has always previously been handled only by specialist fabricators.

**Table 1.2: Weldability of selected non-ASTM Titanium alloys.**

ALLOY GRADE	WELDABILITY	COMMENTS
Ti-6Al-2Sn-4Zr-2Mo	Fair-good	Common aerospace alpha and beta grade
Ti-6Al-2Sn-4Zr-6Mo	Limited	Aerospace alpha and beta grade
Beta III	Excellent	Beta alloy
Ti-15V-3Al-3Sn-3Cr	Excellent	Beta alloy

Over the years, it has been observed that the most likely imperfections in fusion welds are:

- Weld metal porosity.
- Embrittlement.
- Contamination cracking.

### 1.1.1 Weld Metal Porosity

Weld metal porosity is the most frequent weld defect. Jeffus (1997: 493) noted that porosity arises when gas bubbles are trapped between dendrites during solidification. In titanium welding, hydrogen from moisture in the arc environment; or contamination on the filler and parent metal surface, is the most likely cause of porosity. According to the Welding Technology Institute of Australia, ‘it is essential that the joint and surrounding surface areas are cleaned by first degreasing, using steam, solvent, alkaline, or vapour. Any surface oxide should then be removed by pickling (HF-HNO<sub>3</sub> solution), light

grinding or scratch brushing with a clean, stainless steel wire brush' ([www.wtia.com.au](http://www.wtia.com.au)). Fabricators and welders are strongly cautioned not to use ordinary steel brushes because steel brushes would leave some iron particles on the welded surfaces, and cause scratches. These would develop rust and cause, or increase the chances of corrosion.

### **1.1.2 Embrittlement**

Titanium has a very high affinity for oxygen, nitrogen and hydrogen at temperatures above 500°C ([www.twi.co.uk](http://www.twi.co.uk)). Weld metal contamination can cause embrittlement, by either gas absorption or by dissolving contaminants such as dust (iron particles) on the surface. Embrittlement through contamination with air and carbonaceous materials poses a big threat to successful fusion welding of titanium (O'Brien, 1991: 72-86). Hence the area to be welded has to be clean and protected by some inert gas shield while hot. Means of protecting the weldment with inert gas are commercially available and easy to implement. An efficient gas shield can be achieved by welding in an entirely enclosed chamber, filled with the shielding gas, for a small component. The recommendation is that the arc be struck on a scrap piece of titanium, termed 'titanium-getter', before welding to eliminate oxygen from the atmosphere. In tube welding, an entirely enclosed head is equally effective in shielding the weld and is preferred to orbital welding equipment in which the gas nozzle has to be rotated around the tube. When welding in the open, the torch is fitted with a trailing shield to protect the hot weld bead whilst cooling. In this situation, the size and shape of the shield is determined by the joint profile; while its length will be influenced by the welding current and travel speed ([www.wtia.com.au](http://www.wtia.com.au)).

### **1.1.3 Contamination cracking**

If iron particles are present on the component surface, they dissolve in the weld metal causing a reduction in corrosion resistance, and a sufficiently high iron content causes embrittlement ([www.twi.co.uk](http://www.twi.co.uk)). Iron particles are equally detrimental in the heat affected zone (HAZ) where local melting of the particles form pockets of titanium-iron eutectic.

But ordinarily, there is no solidification cracking or hydrogen cracking (Inoue *et al.*, 2002: 56).

## 1.2 Welding

By selecting an appropriate technique in the welding of joints of titanium and its alloys, the favourable properties of titanium; given by its metallurgical characteristics, can be retained or reproduced in the end products. For instance, the oxide film forms equally over welds and heat affected zones as it does over the parent metal. And this film is the basis of the metal's corrosion resistance. Weldments perform identically to their parent metal in corrosion resistant services, except in few very harsh environments (Burges, 1989: 140-142).

Designers select materials with a view of the needs of the eventual products. The constituents of the materials are considered since they could affect the needs of the application of the products. However, the versatility of two basic compositions is such that they continue to satisfy the needs of the majority of applications, and the resulting level of common use remains a major factor in the cost effective production, procurement and application of titanium. These two compositions are commercially pure titanium (ASTM Grade 2) – selected for basic corrosion resistance, with strength in the range of 350 – 450MPa; and high strength titanium alloy (Ti-6Al-4V), with strength in the range of 900 – 1100MPa (Cary & Helzer, 2005: 103-109). Welding consumables are readily available for these grades. Although there are other weldable alloys, consumables for them may need to be obtained from specialist sources (Hass, 2006: 9-10). The full range of titanium alloys starts from high ductility commercially pure titanium, which is used where extreme formability is essential, e.g. in applications such as plate heat exchangers and architectural cladding and roofing; to fully heat treatable alloys, with strength above 1500MPa. Corrosion resistant alloys are capable of withstanding attack in the most aggressive sour oil and gas environments or geothermal brines at temperatures above 250°C. High strength oxidation and creep resistant alloys are used in aero engines at temperatures up to 600°C (Smith *et al.*, 1999: 49-51). Under industrial circumstances

such as these, the welding process employed plays a significant role in ensuring that the performance of titanium fabricated products match or surpass the overall valuable properties of the metal; as required by the target clientele.

To the mutual benefit of the titanium industry and its end users, the improved understanding of welded titanium; and the preservation of its properties after joining, are essential. This will require proper steps towards increased flexibility in material selection and use, modelled to improve quality and performance of the products and processes. This will go a long way to confirming the technical superiority of titanium over other materials, for even more engineering applications than at present.

### **1.3 Problem Statement**

The use of titanium has been hampered by practical challenges in joining it, especially welding (O'Brien, 1991: 66; Michelin, 2010: 213 and [www.wtia.com.au](http://www.wtia.com.au)). The properties of the weld joints and heat affected zones are different from those of the rest of the material not affected by heat due to welding (Askeland, 1996: 423-424 and Porter & Easterling, 1995: 116-117). This difference in properties affects the ability of the different sections of the joined material to withstand load stress (Boyer et al., 1994: 283) equally. Also, the properties of welded titanium alloys were previously not well documented ([www.twi.co.uk](http://www.twi.co.uk)). The high cost of titanium, its alloys, and their production processes have discouraged many potential investors in the past from investing in their development, production and use (Jeffus, 1997: 491-494). Consequently, there has previously been less research work on it either, when compared to other metals and their alloys ([www.timet.com](http://www.timet.com); [www.wtia.com.au](http://www.wtia.com.au) and [www.twi.co.uk](http://www.twi.co.uk)). This situation limits the volume of data available for research purposes, and has not helped engineers, designers and fabricators.

## **1.4 Specific Objectives of the Research**

This research work is undertaken to know if welded titanium (grade 5) alloy pipes would fail under stress caused by fluid flow through pipes in industrial operations. It will contribute towards understanding the distribution of load stress along pipelines. Ti6Al4V alloy pipes' ability to withstand load stress can be determined by ascertaining if they meet the industry acceptable stress limit of materials when put under maximum desired load. So this study will help determine if the weldments along Ti6Al4V alloy pipelines can withstand the effects of load stress during fluid flow. This work will also seek to contribute towards determining the reliability of welded Ti6Al4V alloy pipes in comparison with the unwelded ones. It will contribute towards determining the effect of welding on the properties of Ti6Al4V. It will help to determine the strength differences in joined pipes compared to continuous pipes, as well as the comparison between seam welded pipes and unwelded pipes. Welded titanium alloy pipes, having as much strength as the unwelded alloys at the least, will add a lot of value to the industrial operations of organisations concerned with the flow of fluid. It will contribute towards promoting the use of titanium and its alloys in the production processes of major global economic players like those in the oil and gas sector.

## **1.5 Value of the Research**

Through this work, the use of titanium (grade 5) alloy pipes will be given much consideration in industrial production operations. This work will contribute towards making the science and practice of laying titanium alloy pipes easier to understand by professionals involved in the relevant industries. In so doing, it will place engineers in a better position to design and redesign titanium alloy pipe networks for use in industrial operations; and fabricators will be better equipped to decide on the position of weld joints in pipe networks too. Therefore, the works of the fabricators, welders and artisans will have more value. With such easier understanding of welding positions, the design and laying of titanium alloy pipe networks will become simple to carry out. Less time and energy will be expended on pipe laying and general production processes in which

titanium alloy pipes will be used. This will result in a reduced cost of production. Hence the affected industries will find this material cheaper to use, which will translate into an increase in the value that titanium products will be adding to end users.

It is expected too that the resultant negative effects on the environment of using cheaper alternative materials for pipes, which corrode and fail quicker than those made of titanium alloys will be minimized, if not completely eliminated. Apart from humans, other living things such as aquatic lives and plants suffer the consequences of environmental pollution caused by leakages in fluid pipes e.g. oil spillage and air pollution. These industrial accidents are sometimes as a result of pipe failure caused by corrosion, and/or other properties of the pipe material (Hawkins, 2008: 8518 and Shehata *et al.*, 2008: 117-119). Ti6Al4V pipes will significantly reduce such harmful incidents.

## **1.6 Research Methodology**

A literature study of titanium and its alloys, taking into account their availability, cost of production, use, needs, and importance was reviewed; as a first step in this research. Welding, and the practice of many of the existing welding processes was reviewed too. A review of literature on the welding of titanium and its alloys was also done. Literature on pipes, titanium, the different methods of joining titanium, finite element analysis, and the structural analysis of pipes conveying fluid, was reviewed as well. Stress, strain, displacement, and fatigue analyses of pipe models welded at different positions along their lengths, using Gas Tungsten Arc Welding (GTAW) method, otherwise known as Tungsten Inert Gas (TIG), was done.

A finite element method software, Pro/ENGINEER Wildfire 5.0, which uses the finite element analysis technique was used to develop the pipe models. The same software was used to run structural simulation analyses of the models. The different structural reactions of these models, the data generated from the various simulations run, and the results of these simulations are presented and discussed in this dissertation. The advantages and shortcomings of the pipe models were taken into consideration in the analysis.

Experimental data obtained from on-going scientific and industrial research works were studied as well. Results of the different processes of joining titanium and its alloys with stainless steel, low carbon steel, and many other engineering materials were studied. The results of completed research works relating to the response of pipes to the effects of fluid flow through pipe conduits were used to compare with the results obtained in this work. There were reduced pipe models of every model type, to compare with the “full” models, and to check the accuracy of the finite element analysis. The reduced models were further symmetrically constrained for more detailed analysis. Analytical hoop stress value was calculated, and the von Mises stress results compared to the analytically determined result.

## **Chapter 2 Review of FEA, pipes, welding, titanium, Ti4Al6V, and the joining of titanium.**

### **2.1 Introduction**

In this chapter, the literature on pipes, the practice and science of welding, the different welding processes, tools, materials and environmental conditions is reviewed. The literature on titanium and the methods of joining it is also reviewed. A proper theoretical understanding of existing welding processes, techniques, material composition and other parameters is very crucial for the development of a process model. Research works that contributed to the development of simulations and models of titanium welding processes are reviewed, with the aim of identifying the parameters that influence weld quality; as well as the inter-relationships of these parameters (Cary & Helzer, 2005: 5-9; David, 2003: 1022-1026 and David *et al.*, 2005: 67-91). In this review chapter, attention will be paid to those welding processes that have been employed in the joining of titanium and its alloys, in different industries, and considering their effectiveness under the different environmental conditions. Effects of stress on titanium weldments are reviewed too.

### **2.2 Finite Element Analysis (FEA)**

Finite Element Analysis (FEA) is an approach that uses a numerical technique, the Finite Element Method (FEM) to find approximate solutions to partial differential and integral equations. And FEM is an analytical technique that predicts the responses of some engineering systems to input forces/loads. It is a good method for solving partial differential equations when domains change as is the case when a solid state reacts to a moving boundary, or over complex domains like pipe networks among others (Strang & Fix, 1973: 8). It is used to predict field quantities such as stress, velocity, displacement, and temperature of structures under load. An important characteristic of FEM is meshing – splitting a continuous domain into a finite set of discrete sub-domains known as elements. The elements represent the characteristics of the parent (or continuous) domain, with nodes at their corners or edges, and are connected to one another through those

nodes. The different quantities of interest such as displacement (for structures), pressure (for fluid), or temperature (for heat transfer) are identified at each node; and are used to develop equations based on the equilibrium of the nodes. For structures, the equation will be basically put in the form:

$$\{f\} = [k]\{d\}$$

where

$\{f\}$  = the forces working at the nodes

$\{d\}$  = the displacements at the nodes

$[k]$  = the element stiffness matrix

As the number of elements increases, the number of nodes will increase correspondingly, resulting in more variables and, in effect, more equations to solve. When defined properly, more elements give finite element models that closely represent the true characteristics of the domain (Kuntjoro, 2006: 2-4). In application therefore, many real life domains under FEM analysis have quite a large number of nodal equations. Hence, the use of the computer is necessary in its application.

FEM allows detailed visualization of joints and bends, showing stress distributions and displacements ([www.ptc.com](http://www.ptc.com)). It is used in the engineering design and development of products in major sectors of the global economy such as the automotive, aeronautical, and biomedical industries. A variety of FEM software packages exists, and they integrate a wide range of options to control the modelling, simulation, and analysis of systems. The software packages employ a sequence of three stages in their analysis. The stages are pre-processing, solution process, and post-processing. Pre-processing includes geometric preparation, selection of materials, application of loads, selection of elements, discretization of the domain, and the specification of the boundary conditions and constraints. Based on the pre-processing, the software automatically sets up the equilibrium equations internally. These equations are then solved in the solution process to produce the field values at the nodes. Post-processing is the presentation of the analysed parameters (Kuntjoro, 2006: 2-4). This analysis allows the entire products' designs to be constructed, refined, and optimized before they are manufactured. And this

has significantly reduced the time taken to see products from their concept to the production line. FEM enhances product design and accuracy, reducing the number of hardware prototypes of products, and resulting in a faster and less expensive design cycle. The FEM software package used for this work - Pro/ENGINEER Wildfire 5.0 gives very good simulation results for structural (static and fatigue) design studies.

### 2.3 Pipes

Pipes are hollow cylinders used to convey fluid substances over distances. When many pipes are joined together, they form a network. Pipe networks are commonly used to move fluid from one point to another. They are made of materials with good properties to avoid any damages that would arise if they fail, or are tampered with. Therefore, pipes made of titanium alloys may be very reliable, considering the metal's good properties.

McAllister (2005: 44) pointed out that at present, fluids conducted via pipes over long distances include water, crude oil and fuel products such as paraffin oil (kerosene), premium motor spirit (petrol), diesel, methane gas, marine fuel, and other petroleum products. Pipes have specific sizes and standard designations. They may be manufactured according to Nominal pipe sizes or by Outside diameter (OD) and wall thickness, depending on industrial and government regulations ([www.vogeltool.com](http://www.vogeltool.com)). In practical applications, pipeline systems in different geographical locations would differ in purpose, operating environment, economic conditions, regulatory requirements, complexity, size, and design philosophy (Kennedy, 1993: 5). Though costs for offshore pipelines are significantly higher than the costs of pipelines on land, it is generally agreed that the longer the pipeline, the lower the cost per kilometer; except in extreme environments such as the Arctic or mountainous regions. For instance, a pipeline measuring a few kilometers long usually costs considerably more per kilometer than a pipeline several hundreds of kilometers long, even if both pipelines are of the same diameter and are laid in a similar environment (Kennedy, 1993: 15-18). Therefore, fluid conduit operators would be better off using pipelines made of reliable engineering materials very extensively.

## **2.4 Welding**

Fabrication using high tonnage metal components invariably requires joining in some form, and the metal should have the ability to be joined to itself and to other metals. These joining methods include welding, brazing, soldering, riveting and bolting. Titanium therefore, like any other metal, requires joining in order to be a useful structural metal for such applications as in aircrafts, bridges, pipes, tanks, vehicles, and ships. Moreover, for a joint to be useful, it must possess mechanical properties which meet the service requirement specifications of the end product (Elmer & Wong, 2001: 1-11). Presently, increasing scientific research and development of the techniques of titanium joining have reduced a previously seeming insurmountable problem to one of practical solution with precautionary techniques ([www.keytometals.com](http://www.keytometals.com)). One of the most resourceful activities in the world is welding. It is a fabrication process that is used to join materials, usually metals or thermoplastics, by causing coalescence. Welding often requires the use of heat, pressure or both, in the melting of a material before joining it to another material. It could be by autogenous melting of the workpieces and adding a filler material to form a pool of molten material (the weld puddle) that cools and solidifies to become a strong joint, but sometimes pressure is used in conjunction with heat, or by itself, to produce the weld (Weman, 2003: 31-38).

The most widely used method of joining metals is welding. In comparison with other joining methods such as riveting and bolting, it is stronger, weighs lighter, and is less expensive. Welds hold together much of the joined materials and parts that are made to become heavy industrial equipment and facilities the world over. They make possible, metal bridges, office buildings, and high-pressure tanks; as well as all sorts of high-technology devices. Our safety while driving in cars, flying in aircrafts, sailing in ships etc; depend in part, on the reliability of more than 3,000 welds (Elmer & Wong, 2001: 2). The results could be catastrophic if a weld were to fail in most practical applications.

The most common method employed in joining titanium, like most other metals in industrial application, is welding. Though there were lots of difficulties at attempts to

weld titanium initially, such problems can be overcome with the application of proper techniques, owing to extensive experiments and scientific investigations. Provided the beta content is not too high, and additional contamination is not caused by the surrounding atmosphere too; a sound weld with good properties as-welded, can be achieved by selecting materials of low interstitial content, as the chemical analysis of such selected materials would show (Danielson *et al.*, 2003: 2-7). The careful choice of such titanium alloy composition and welding parameters will result in sound welds embodying ductility, resistance to impact loading, and strength (Donachie, 2000: 6-13 and ([www.keytometals.com](http://www.keytometals.com))).

With low interstitial content, unalloyed titanium is readily weldable. However, the typical alpha-beta alloys, containing manganese, chromium, iron, vanadium, and molybdenum; when welded, usually have a much lower bend ductility and notch toughness. Bend ductility and notch toughness decrease severely as the total alloy content of beta stabilizing elements increases. Such alloys may contain amounts of the alpha stabilizers, aluminum and tin, to permit greater alloy content without further loss of ductility. Beta alloys are lean in alpha stabilizers, rich in beta stabilizers, so that the beta phase can be completely retained with appropriate cooling rates. They are unstable, and can be strengthened by the precipitation of alpha phase, though they are higher in density than comparable alpha-beta alloys (Danielson *et al.*, 2003: 2-7 and Donachie, 2000: 6-13).

Over the years, the materials used by welders have changed. Today, they include not just metals but also polymers, ceramics, and composites. Lasers, electron beams, and plasma arcs supplement traditional electric and torch welding methods. Yet for all this history, sufficient knowledge about titanium welding processes is surprisingly sparse, when compared to the welding processes of other metals. For instance, forge welding has been around almost since people began to work with metals. In the late 19th century, Sir Humphrey Davy discovered the electric arc, and modern welding was born (Elmer & Wong, 2001: 1). According to [www.azom.com](http://www.azom.com), such conventional welding methods and inspection techniques are not adequate for predicting a weld's evolution in time. Welding may be old, but the science of welding is still developing.

When two pieces of material are being welded together, high heat rapidly melts the solid material. It then quickly cools and solidifies again as the heat source moves away. Adjacent to the immediate weld area, or fusion zone, is the heat-affected zone (HAZ). As the name HAZ implies, the material there is affected by the high heat of the welding process but does not melt, though some degree of heat causes microstructural changes in materials. Elmer and Wong (2001: 4) and David *et al.* (2005: 67-81) noted that when a material is welded, the applied heat causes phase change, due to the change(s) in the crystalline structure of the material. These microstructural changes can affect the strength of the material as well as its corrosion resistance, ductility, and mechanical properties. The quality (or integrity) of the weld therefore, can either be enhanced or reduced by any or all of these changes. A very clear understanding of such changes will help to predict their occurrences. Hence real experimental data during welding are needed, to increase an understanding of the details of such welding processes.

#### **2.4.1 Welding processes**

Commercially pure titanium and most titanium alloys can be welded by procedures and equipment used in welding austenitic stainless steel and aluminum. They are joined by various fusion-welding processes. Some of such processes include:

- Gas-tungsten arc welding (GTAW)
- Gas-metal arc welding (GMAW)
- Plasma arc welding (PAW)
- Electron-beam welding (EBW)
- Laser-beam welding (LBW)
- Friction welding (FRW)
- Resistance welding (RW)

Other welding processes like electroslag welding, submerged arc welding, flux-cored arc welding also exist. Though these processes are very useful in many industrial applications, this research will not pay particular attention to them, but to the commonly applied gas-tungsten arc welding (GTAW). Fluxes cannot be used with any of GTAW,

GMAW, PAW, EBW, LBW, FRW and RW processes because they combine with titanium to cause brittleness, and possibly, reduced corrosion resistance too.

#### **2.4.1.1 Gas-tungsten arc welding (GTAW)**

This is also known as Tungsten Inert Gas (TIG) welding. It is an arc welding process that uses a non consumable tungsten electrode to produce the weld. The weld area is protected from atmospheric contamination by a shielding gas (usually an inert gas such as argon or helium), and a filler metal is normally used, though some welds, known as autogenous welds, do not require it. A constant-current welding power supply produces energy which is conducted across the arc through a column of highly ionized gas and metal vapors known as plasma (Sista *et al.*, 2000: 4813-4825).

GTAW is most commonly used to weld thin sections of stainless steel and light metals such as aluminium, magnesium, copper alloys, and titanium. The process grants the operator greater control over the weld than competing processes such as shield metal arc welding and gas metal arc welding; allowing for stronger, higher quality welds. However, GTAW is comparatively more complex and difficult to master, and furthermore, it is significantly slower than most other welding techniques, even though it is low on capital and running costs (Minnick & William, 1996: 84). Among arc welding processes, GTAW ranks the highest in terms of the quality of weld produced. Maximum quality is assured by maintaining cleanliness during operation – all equipment and materials used must be free from oil, moisture, dirt and other impurities; as these cause weld porosity and consequently a decrease in weld strength and quality.

GTAW is the most widely used process for joining titanium and titanium alloys except for parts with thick sections. Tables 2.1 to 2.2 give the bend strength of materials that can be used in GTAW processes and the type of weld that will result from the process. Square-groove butt joints can be welded without filler metal, in base metals with thickness of up to 2.5mm. For thicker base metals, the joint should be grooved, and filler

metal is required. Tables 2.3 show the impurity content, in percentage by weight, of Commercially Pure titanium filler materials (Danielson *et al.*, 2003: 2-7).

**Table 2.1: Bend Strength of Materials and Welds.**

Bend Strength MPa (ksi)	CP-Ti (Filler) Rod	CP-Ti Plate	Low Oxygen Weld	High Oxygen Weld
	N/A	109 (16)	73.3 (10.6)	27.5 (4.0)

**Table 2.2: Types of Weld.**

TYPE OF WELD	IMPURITY CONTENT (wt%)		
	Oxygen	Nitrogen	Carbon
Low Oxygen Weld	0.190	0.050	0.019
High Oxygen Weld	0.437	0.392	0.038

**Table 2.3: Impurity content (wt%) of CP-Ti filler materials.**

WELD (MATERIAL)	FILLER	Oxygen	Nitrogen	Carbon
CP-Ti (Filler) Rod		0.189	0.001	0.029
CP-Ti Plate		0.189	0.007	0.021

During GTAW process, the heated weld metal in the weld zone should be shielded from the atmosphere to prevent contamination with oxygen, nitrogen, and carbon, which will degrade the weldment ductility (Minnick & William, 1996: 83-84).

Though gas tungsten arc welding is most commonly used to weld stainless steel and nonferrous materials, such as aluminium and magnesium, it can be applied to nearly all metals, with notable exceptions being lead and zinc. Its applications involving carbon steels are limited not because of process restrictions, but because of the existence of more economical steel welding techniques, such as gas metal arc welding and shield metal arc welding (Folkhard *et al.*, 1987: 52).

#### **2.4.1.2 Gas-metal arc welding (GMAW)**

This is used to join titanium and titanium alloys with thickness of more than 3mm. It is applied using pulsed current or the spray mode and is less costly than GTAW, especially when the base metal thickness is greater than 13mm. It is sometimes referred to, by its subtypes – metal inert gas (MIG) welding or metal active gas (MAG) welding. It is a semi-automatic or automatic arc welding process in which a continuous and consumable wire electrode and a shielding gas are fed through a welding gun. A constant voltage, direct current power source is most commonly used with GMAW, but constant current systems, as well as alternating current, can be used. Generally, it is unsuitable for welding outdoors, because the movement of the surrounding atmosphere can cause the dissipation of the shielding gas and thus make welding more difficult, while also decreasing the quality of the weld. The problem can be alleviated to some extent by increasing the shielding gas output, but this can be expensive. The four primary methods of metal transfer in GMAW are globular, short-circuiting, spray, and pulsed-spray. Each of which has distinct properties and corresponding advantages and limitations (Weman, 2003: 97-98).

In most of its applications, gas metal arc welding is a fairly simple welding process to learn, requiring no more than several days to master the basic welding technique. However, even when performed by well trained operators, the weld quality can fluctuate, since it depends on a number of external factors. All GMAW operations are dangerous, though perhaps less so, than some other welding methods.

#### **2.4.1.3 Plasma arc welding (PAW)**

Plasma arc welding is an advancement over the GTAW process. It is also applicable in joining titanium and titanium alloys (Yang *et al.*, 2000: 177-181). This is an arc welding process similar to gas tungsten arc welding (GTAW). The electric arc is formed between an electrode (which is usually but not always made of a sintered tungsten) and the workpiece. The key difference from GTAW is that in PAW, the electrode is positioned

within the body of the torch. This separates the plasma arc from the shielding gas envelope. The plasma is then forced through a fine-bore copper nozzle which constricts the arc and the plasma exits the orifice at high velocities (approaching the speed of sound) and a temperature approaching 20,000 °C. It is faster than GTAW and can be used on thicker sections such as one-pass welding of plates that are up to 13mm thick, using keyhole techniques (Weman, 2003: 127-128).

This process uses a non-consumable tungsten electrode and an arc, constricted through a fine-bore copper nozzle. PAW can be used to join all metals that are weldable with GTAW (i.e., most commercial metals and alloys). Several basic PAW process variations are possible by varying the current, plasma gas flow rate, and the orifice diameter. It has a greater energy concentration than GTAW, though PAW requires relatively more expensive and complex equipment. Proper torch maintenance in PAW is very critical and welding procedures tend to be more complex and less tolerant to variations in fit-up, etc.

#### **2.4.1.4 Electron-beam welding (EBW)**

This is used in the aircraft and aerospace industries for producing high-quality welds in titanium and titanium alloy plates, ranging from 6mm to 75mm thick. It is a fusion welding process in which a beam of high-velocity electrons are applied to the materials being joined. Since the electrons are in motion, they possess kinetic energy. And as the kinetic energy of the electrons is transformed into heat upon impact, the work pieces melt. The filler metal too, if used, melts to form part of the weld. Pressure is not applied, and a shielding gas is not used, though the welding is always done in a high vacuum chamber to prevent dispersion of the electron beam (Yunlian *et al.*, 2000: 177-181).

In this process, according to Cary & Helzer (2005: 202-206), the electrons strike the workpiece, instantly vaporizing the metal under temperatures near 25,000°C. The heat therefore penetrates deeply, making it possible to weld much thicker workpieces than is possible with most other welding processes. However, the total heat input is actually much lower than that of any arc welding process, because the electron beam is tightly

focused. As a result, the effect of the welding; on the surrounding material is minimal, and the heat-affected zone is small (Chaturvedi *et al.*, 1999: 130-134). The distortion here is slight, and the workpiece cools rapidly. In this welding process, the amount of heat input, and thus the penetration, depends on several variables, most notably the number and speed of electrons impacting on the workpiece, the travel speed, and the diameter of the electron beam. Greater beam current causes an increase in heat input and penetration, while higher travel speed decreases the amount of heat input and reduces penetration. The diameter of the beam can be varied by moving the focal point with respect to the workpiece - focusing the beam below the surface increases the penetration, while placing the focal point above the surface increases the width of the weld. Since the welding is performed in a high-vacuum atmosphere, low contamination of the weldment is achieved.

EBW is very suitable for the welding of CP-Ti sheets. Using this process, the welding seam can be obtained without defects (Yunlian *et al.*, 2000: 179). EBW can be employed in the joining of Ti Al-based alloys, though with solid state cracking, due to the intrinsic brittleness of the microstructure, and the high thermally induced stresses (Schultz & Helmut, 1993: 72). With careful selection of welding parameters, using the continuous cooling transformation (CCT) diagrams of the materials to be welded as guide, crack-free welds can be obtained. This way, the microstructural changes are controlled, and in effect, the cracking susceptibility of the welds (Chaturvedi *et al.*, 1997: 239-240).

#### **2.4.1.5 Laser-beam welding (LBW)**

In this technique, a laser beam is used to join multiple pieces of metal. The beam provides a concentrated heat source, allowing for narrow, deep welds and high welding rates. The process is frequently used in high volume applications. It is increasingly being used to join titanium and titanium alloys. Square-but weld joint configurations can be used, and the welding process does not require the use of vacuum chambers, although gas shielding is still required. According to Smith *et al.* (1999: 8) this process is more limited than electron-beam welding regarding base metal thickness, which usually cannot exceed

13mm. Yet, like electron beam welding, it has high power density (on the order of 1 MW/cm<sup>2</sup>) resulting in small heat-affected zones, and high heating and cooling rates. The spot size of the laser beam can vary between 0.2 mm and 13 mm, though only the smaller sizes are used for welding. The depth of penetration is proportional to the amount of power supplied, but is also dependent on the location of the focal point. The penetration is maximized when the focal point is slightly below the surface of the workpiece.

LBW is a versatile process, capable of welding titanium and other metals and alloys such as carbon steel, stainless steel and aluminum. The weld quality is high, and similar to that of electron beam welding. The speed of welding depends on the amount of power supplied, and on the type and thickness of the workpieces too. The high power capability of laser beam welders makes them especially suitable for high volume applications (Weman, 2003: 97-98).

#### **2.4.1.6 Friction welding (FW)**

Friction welding is a group of solid-state welding processes where heat generated through mechanical friction between moving workpieces is used, with the addition of an upsetting force, to plastically displace the metal at the weld. It involves holding two components in axial alignment. In FW, there are a number of process variations, and many dissimilar metal combinations can be joined. This process is useful in joining tubes, pipes, or rods, where joint cleanliness can be achieved without shielding. At high temperatures such as those used for joining titanium, all heat treating atmospheres contain some hydrogen; except in cases where inert gases, salt baths or high vacuum are employed. The presence of hydrogen could be as a result of the breakdown of water vapour when an electric furnace is used under air atmosphere, or even as a by-product of incomplete combustion in the use of hydrocarbon fuel (Donachie, 2000: 9-12, 337). Since welding involves more than one alloy or material, titanium hydrides are formed along the weld interface when hydrogen migrates from one alloy to another (Fuji, *et al.*, 2001: 26). Hydrogen contributes to the embrittlement of the weld. Adams (1958: 210) stated that the

embrittlement of titanium alloys by hydrogen is difficult to avoid, especially when dissimilar alloys are welded to each other. When theoretical considerations are made, the combined effects of hydrogen diffusion in metals are considered, because they affect the gradient in interstitial concentration, temperature, stress, and solvent composition. As in most other solids, Fick's laws describe the diffusion problems in metals. The most applicable one being:

$$J = -D(dC/dx) = -D\Delta C \quad 2.1$$

where,

J is the flux of diffusing atoms

C is the concentration

D is the diffusion coefficient.

There are many types of friction welding processes. Some of the processes (techniques) are used in joining metals, and there are others used in joining thermoplastics. In this dissertation, the different types of friction welding will not be treated in detail. However, they include the following, two of which will be reviewed as sample FW techniques.

- Linear friction welding
- Friction stir welding
- Spin welding
- Friction surfacing
- Linear vibration welding
- Orbital friction welding
- Angular friction welding and
- Inertia friction welding

Figure 2.1 illustrates the principle employed in the friction welding process (Sluzalec, 1988: 53).

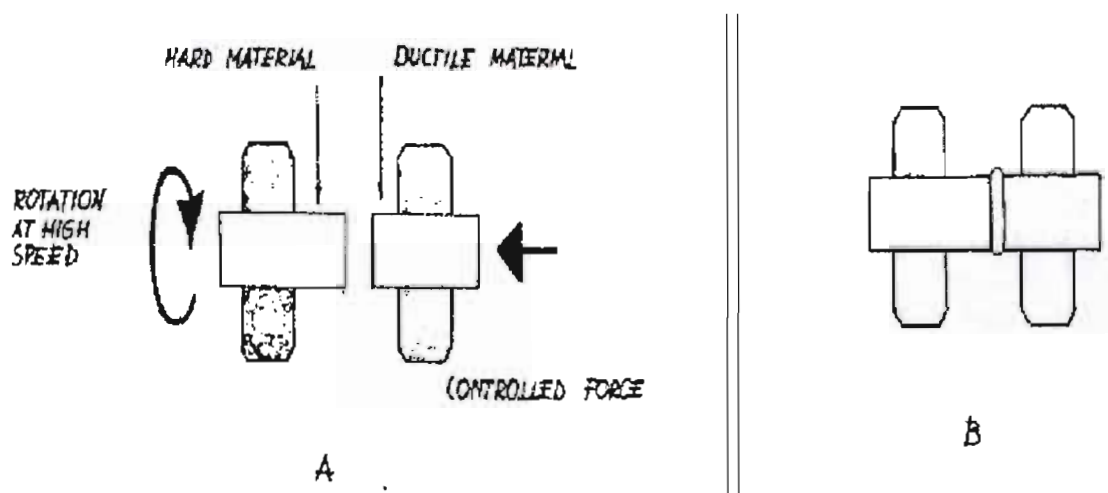


**Figure 2.1: Principle of friction welding process. (A) Store kinetic energy in flywheel and apply controlled end force. (B) Rotation ceases and weld is complete (Sluzalec, 1988: 53).**

#### 2.4.1.6.1 Linear Friction Welding (LFW)

Linear Friction Welding (LFW) is a solid phase, machine tool based process that is used in joining complex geometry components. It involves the use of linear reciprocating motion, where a component is rubbed across the surface of another rigidly clamped component. It is seen as a key technology for the aerospace industry as it enables the joining of materials that are ordinarily difficult to bond. It can be used to build the complex structures required for today's gas turbines, and as a repair process as well. Essentially, it is a non-melting joining process producing high integrity welds, requiring little prior surface preparation (Threadgill, 2008: 335-340).

According to Vairis & Frost (2000: 8-17), when the parts to be welded are forced into intimate contact, a fully reversed motion is imposed on parts of the system. This generates frictional heat in the immediate region about the weld plane, thereby softening a finite volume of the material. As the weld proceeds, a portion of this visco-plastic layer is extruded at the periphery of the weld interface, in rippled sheets of metal known as

flash. This should ensure that any interfacial contaminant is expelled. The combination of fast joining times of the order of a few seconds, and the direct heat input at the weld interface, gives rise to relatively small heat affected zones; which effectively limits process induced distortions. However, some judicious selection of components' geometry has to be applied.

Though very little research has been done in the area of LFW, it is generally accepted that friction welding can be separated into three possible stages, namely:

- (i) A dry friction stage
- (ii) An increased asperity contact
- (iii) Some sort of steady state, once the relatively high weld temperature has been acquired.

However, it is not clear how surface contaminants are removed, especially from the mid-point of the weld.

#### **2.4.1.6.2 Friction Stir Welding (FSW)**

Friction stir welding (FSW) is a novel welding technique invented by The Welding Institute (TWI) in 1991. FSW is actually a solid-state joining process that is a combination of extruding and forging and is not a true welding process (Smith *et al.* 1999: 49). Smith *et al.* (1999: 52-57) concluded that FSW has several advantages over fusion welding, including energy efficiency and minimal usage of consumables. Also, it produces desirable microstructures in the weld and heat-affected zones. It is environment friendly (no fumes, noise, or sparks), has the ability to successfully join materials that are "unweldable" by fusion welding methods, and produces less distortion than fusion welding techniques. These are due to the fact that the process occurs at a temperature below the melting point of the work piece material. The tensile properties of friction stir welded Ti-6Al-4V are shown on table 2.4. Friction stir welding uses a cylindrical, shouldered tool with a profiled pin that is rotated and slowly plunged into the joint line between two pieces of sheet or plate material, which are butted together. Frictional heat is

generated between the wear resistant welding tool and the work piece. This heat causes the work piece material to soften without reaching the melting point and allows the tool to traverse the weld line (Russell, 2003:3). As it does, the plasticized material is transferred from the leading edge of the tool to the trailing edge of the tool shoulder and pin. It leaves a solid phase bond between the two work pieces.

**Table 2.4: Tensile properties of selected welds in 6.35 mm thickness of Ti-6Al-4V (Russell, 2003:4).**

SAMPLE NUMBER	SECTION AREA (mm <sup>2</sup> )	MAXIMUM LOAD (kN)	MAXIMUM STRESS (N/mm <sup>2</sup> )	ELONGATION (%)
Parent	-	-	1335.0	14.0
w5.7A	66.0	67.3	10.2	8.5
w5.7B	65.7	64.8	986.0	8.5
w5.18A	60.2	64.3	1068.0	8.0
w5.18B	61.2	65.1	1064.0	7.5

#### **2.4.1.7 Resistance welding (RW)**

This is used to join titanium alloy sheet and other metals by either spot welds or continuous seam welds, according to Shigley (1986: 353). It is also used for welding titanium sheet to dissimilar metals, that is, cladding titanium to carbon or stainless steel plate. RW refers to a group of welding processes that produce coalescence of faying surfaces, where heat to form the weld is generated by the resistance of the welding current, through the workpieces. Some of the factors that influence the heat or the welding temperatures are the proportions of the workpieces, the electrode materials, electrode geometry, electrode pressing force, weld current and weld time, etc. Small pools of molten metal are formed at the point of the highest electrical resistance (the connecting surfaces) as a high current (100–100 000A) is passed through the metal. Generally, resistance welding methods are efficient and cause little pollution to the

environment, but their applications are limited to relatively thin materials and the equipment cost can be high (David *et al.*, 2005: 85-91).

## **2.5 Filler material and electrodes**

### **2.5.1 Filler-metals**

Metals added in the making of a joint through brazing, soldering, or welding are filler metals. Filler-metal composition is usually matched to the grade of titanium being welded. For improved joint ductility in welding the high strength grades of Commercially Pure titanium, filler metal of yield strength lower than that of the base metal is occasionally used. Because of the dilution that occurs during welding, the weld deposit acquires the required strength. Unalloyed filler metal is sometimes used to weld Ti-5Al-2.5Sn and Ti-6Al-4V for improved joint ductility ([www.timet.com](http://www.timet.com)). The use of unalloyed filler metals lowers the beta content of the weldment, thereby reducing the extent of the transformation that occurs and improving ductility. However, the approval of an experienced fabricator is recommended, when using pure filler metal to ensure that the weld meets strength requirements (Donachie, 2000: 4-5).

Another option is filler metal containing lower interstitial content (oxygen, hydrogen, nitrogen, and carbon) or alloying contents that are lower than the base metal being used. The use of filler metals that improve ductility does not preclude embrittlement of the HAZ in susceptible alloys. In addition, low-alloy welds may enhance the possibility of hydrogen embrittlement.

### **2.5.2 Shielding gases**

Shielding gases in welding titanium and titanium alloys are argon and helium, and occasionally; a mixture of these two gases is used for shielding. However, argon is more widely used; just because it is more readily available and less costly as well.

### 2.5.3 Electrodes

The American Welding Society and the International Organisation for Standardization have standardized a number of tungsten alloys in AWS A5.12 and ISO 6848 respectively; for use in GTAW electrodes. Tungsten's melting temperature of 3,410°C is the highest among pure metals, hence, electrodes used in GTAW are made of it or its alloys (Weman, 2003: 31-38). Table 2.5 below, gives a summary of standardized tungsten alloys, for use in GTAW electrodes.

Due to the high melting temperature of tungsten, it is not consumed during welding, even though some burn-off (erosion) can occur. Electrodes can either be clean finished – when they are chemically cleaned, or ground finished – when they have been ground to a uniform size and their surfaces polished.

**Table 2.5: Tungsten alloys, for use in GTAW electrodes** (Minnick & William 1996: 84).

ISO Class	ISO Colour	AWS Class	AWS Colour	Alloy
<i>WP</i>	Green	EWP	Green	None
<i>WC20</i>	Gray	EWCe-2	Orange	2%CeO <sub>2</sub>
<i>WL10</i>	Black	EWLa-1	Black	1%La <sub>2</sub> O <sub>3</sub>
<i>WL15</i>	Gold	EWLa-1.5	Gold	1.5%La <sub>2</sub> O <sub>3</sub>
<i>WL20</i>	Sky-blue	EWLa-2	Blue	2%La <sub>2</sub> O <sub>3</sub>
<i>WT10</i>	Yellow	EWTh-1	Yellow	1%ThO <sub>2</sub>
<i>WT20</i>	Red	EWTh-2	Red	2%ThO <sub>2</sub>
<i>WT30</i>	Violet			3%ThO <sub>2</sub>
<i>WT40</i>	Orange			4%ThO <sub>2</sub>
<i>WY20</i>	Blue			2%Y <sub>2</sub> O <sub>3</sub>
<i>WZ3</i>	Brown	EWZr-1	Brown	0.3%ZrO <sub>2</sub>
<i>WZ8</i>	White			0.8%ZrO <sub>2</sub>

## **2.6 Titanium**

Titanium and its alloys have very good physical properties - high strength, low density, good creep resistance of up to about 550°C, corrosion resistance, among others (Barksdale & Jelks, 1968:738; Boyer *et al.*, 1994: 346; Clark & Varney, 1965: 52-57 and [www.timet.com](http://www.timet.com)). Practical and comparative welding processes have shown that over time, titanium provides technical and economic advantages in a wide range of production processes, in many high investment industries ([www.timet.com](http://www.timet.com), 2005 and Boyer *et al.*, 1994:483-489).

The light weight and flexibility of titanium pipes make it an excellent material for deep sea production risers in petroleum exploration and production. The world over, it is the preferred material in desalination plants because it shows virtually no corrosion in sea water. And since it shows immunity to attack by sea water, it is the material of choice for topside water management systems ([www.timet.com](http://www.timet.com)). In the aerospace industry, titanium is used in the manufacture of airframe structure, billet and bar, and for critical jet engine rotating applications like fan blade plates; mainly due to its elevated temperature properties, corrosion resistance, toughness, good fatigue strength, high rigidity-to-weight ratios, and outstanding strength-to-weight ratios (Donachie, 2000:10). In industrial application, this favourable density means that the differential cost of material required for production is reduced, when equipment costs are considered in 'per unit area' of measurement, rather than in 'per unit kilogram'. In other words, less titanium material is required to do the same job, based on strength, than those of its competitors – ferrous and nickel based metals. Furthermore, when titanium is used properly, the only criteria needed to specify any system's wall thickness are pressure and structural requirements; as titanium would not require any corrosion allowance. And because it is very resistant to corrosion, the resultant lower failure rates give reduced downtime, less maintenance and total low cost ([www.timet.com](http://www.timet.com)).

Apart from the industries mentioned above, titanium is being put to very significant use in some other sectors of human endeavour. Such sectors include the military – where titanium's strength-to-weight ratio and superior ballistic properties make it well suited for armour application; medical – for medical replacements such as knee and hip implants, because it is completely inert to human body fluids; sports – for bicycles and golf club heads because of its light weight. Titanium and its alloys are also very useful in architecture because of their resistance to corrosion, environmental inertness, light weight, high strength and low thermal expansion, which are very good attributes of materials considered in architectural designs (Boyer *et al.*, 1994: 483-489).

## 2.7 Ti6Al4V

Presently, Ti6Al4V contributes more than fifty percent of all titanium tonnage used globally, according to [www.timet.com](http://www.timet.com). This alloy of titanium is known for its high strength at low to moderate temperatures, having a high strength-to-weight ratio, stability at temperatures up to 400°C (750°F), excellent mechanical properties, and good corrosion resistance (Smallman & Ngan, 2007: 341-345). This alloy is used in the aerospace industry in the manufacture of airframes, turbine engines, and other engine components such as discs, blades and wheels. Since the alloy has good diffusion-bonding characteristics, it enables the fabrication of complex structures, when combined with superplastic forming (Campbell, 2006: 120-132). Castings of titanium (grade 5) alloy are used as boosters to the external tanks, and to attach the main external fuel tanks to Space Shuttles. In the petrochemical industry, it is used as a major material in the fabrication of heat exchangers (Askeland, 1996: 427-431). Due to the fast growing high cost of oil, and its importance as a primary source of energy globally, the application of titanium and its alloys as material for pipes and tanks in the oil and energy sector is enjoying a lot of attention (Chabak, 2010: 8-9 and Tivelli, 2004: 10-14).

## 2.8 Titanium welding

In practical applications, many pipes are joined together in order to have an effective piping system to facilitate the flow of fluid to the desired points. Welding is a very good technique of joining pipes. Previous works by Kalpakjian (1989: 38-40) and Fuji *et al.*, (2001: 25-29) show that welding has the potential of affecting material properties. Generally, welding increases strength and hardness, while decreasing the tensile properties and (bend) ductility of materials. In all types of welds, contamination by interstitial impurities such as oxygen and nitrogen must be minimized, to maintain useful ductility in the weldment. Alloy composition, welding procedure, and subsequent heat treatment are highly important in determining the final properties of welded joints (Smith, 1981: 51-63). All alloys, including titanium alloys, can be joined by solid state processes. The weldability of titanium alloys is usually assessed on the basis of the toughness and ductility of the weld metal (Hass, 2006: 5). Titanium grade 5 alloy may be joined by any of the wide variety of conventional fusion and solid-state processes, although its chemical reactivity would require some particular measures and procedures (Boyer *et al.*, 1994: 491-494).

Gas Tungsten Arc Welding (GTAW) has been the preferred technique for welding titanium because among arc welding processes, it ranks highest in terms of the quality of weld produced (James *et al.*, 2005: 64-65). More so, GTAW is currently the most widely used process for joining titanium and titanium alloys industrially (James *et al.*, 2005: 62). Hence it had to be the process considered ahead of the rest. The GTAW process grants the operator greater control over the weld than competing processes, since it is significantly slower than most other welding techniques. It is a welding process that is low on capital and running costs. And with proper procedures, extreme cleanliness – to avoid porosity and weld cracking; Ti6Al4V may be welded very successfully using this technique (Porter & Easterling, 1995: 113). The quality of the weld will be appreciably higher when all equipment and materials used are free from oil, moisture, dirt and other impurities (James *et al.*, 2005: 63 and Porter & Easterling, 1995: 114-115).

## 2.9 The heat affected zone

Thermal effects from welding cause metallurgical and mechanical changes in materials. Distortion, grain growth, residual stresses, recrystallisation, and other changes in mechanical properties, may occur due to changes in the microstructure of the materials under analysis (Askeland, 1996: 428-429). The phase diagrams in Figures 2.2, 2.3 and

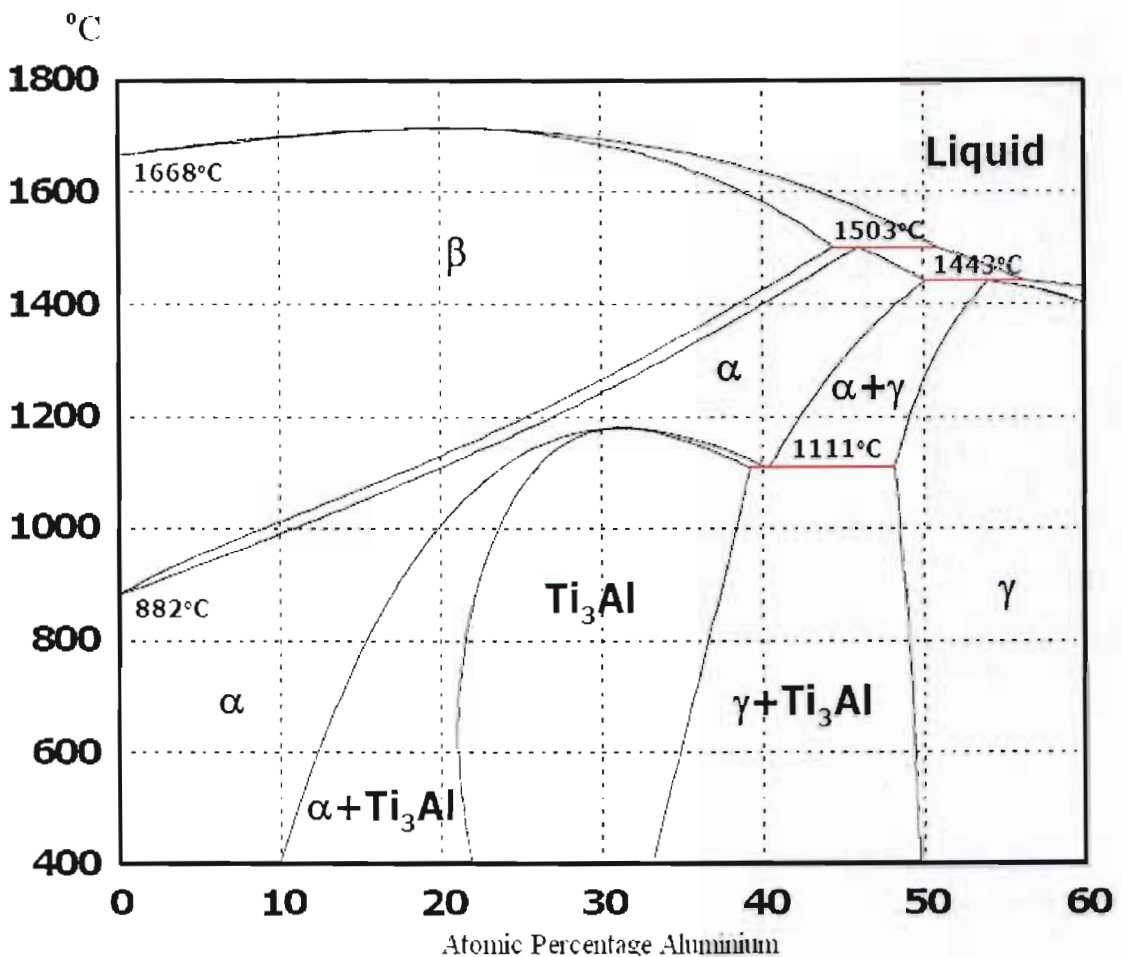


**Figure 2.2: The Titanium Aluminium Phase Diagram (expressed in atomic percent)**  
(Smith, 1981: 51)

2.4 illustrate the resultant effect on the phase composition and microstructure of the sections of the materials affected by the heat (due to the welding), which causes various phase transformations within such portions of the material. Therefore, the mechanical

properties and microstructure of the heat affected zone become different from those of the parent materials (Porter & Easterling, 1995: 116-117).

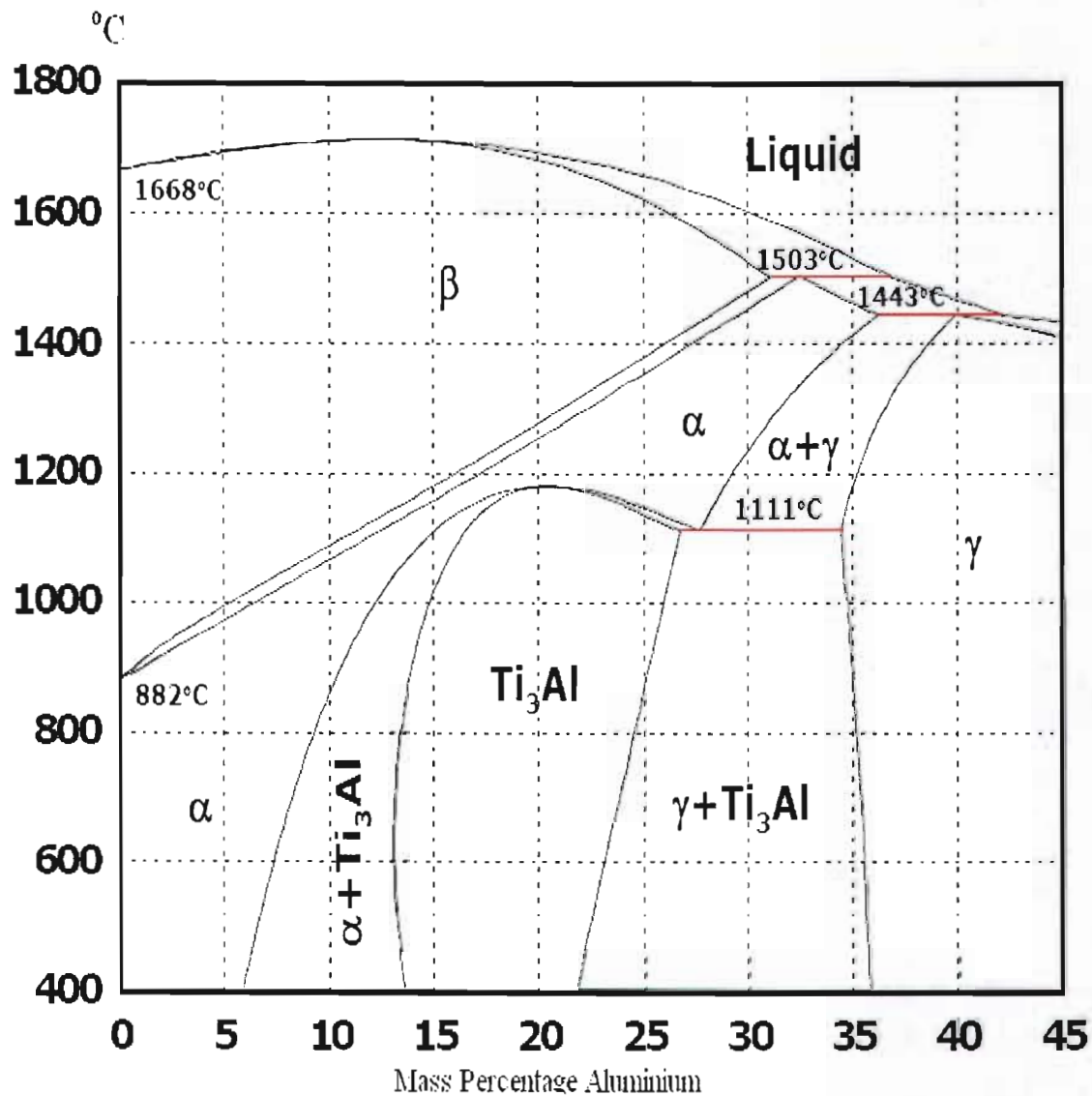


Figure 2.3: The Titanium Aluminium Phase Diagram (expressed in weight percent). (Smith, 1981: 54).

Mathematically, the width of the heat affected zone is calculated using the formula (Adams, 1958: 210):

$$\frac{1}{T_p - T_o} = \frac{4.13\rho CtY}{H_{net}} + \frac{1}{T_m - T_o} \quad 2.2$$

where

$Y$  = the width of the heat affected zone

$T_p$  = the peak or maximum temperature ( $^{\circ}\text{C}$ ), at a distance,  $Y(\text{mm})$ , from the weld fusion boundary.

$T_o$  = initial uniform temperature of the material ( $^{\circ}\text{C}$ )

$T_m$  = melting temperature ( $^{\circ}\text{C}$ ) [specifically, liquidus temperature of the metal being welded]

$H_{net}$  = net energy input =  $\frac{f_lEI}{V}$ , J/mm

[ $E$  = volts;  $I$  = amperage;  $f_l$  = heat transfer efficiency;  $V$  = travel velocity of heat source]

$\rho$  = density of material, g/  $\text{mm}^3$

$C$  = specific heat of solid metal, J/g .  $^{\circ}\text{C}$

$\rho C$  = volumetric specific heat,  $\text{J}/\text{mm}^3 \cdot ^{\circ}\text{C}$

$t$  = thickness of sheet or plate, mm

[It should be noted that the above equation does not apply within the weldment, but only in the adjacent heat affected zone].

At  $Y = 0$ , the equation shows that  $T_p = T_m$

This is consistent with the requirement that the peak temperature at the weld fusion boundary equals the melting temperature. The peak temperature decreases with increasing distance from the weldment because heat decreases with increasing distance from its source.

By increasing or decreasing the input energy, and the volume of material (metal) heated above certain temperatures, the width of the heat affected zone can be controlled. Apart from determining the width of the heat affected zone, the formula can also be used to:

- Show the effect of pre-heat on the width of the heat affected zone; and
- Determine the peak temperatures at specific locations within the heat affected zone.

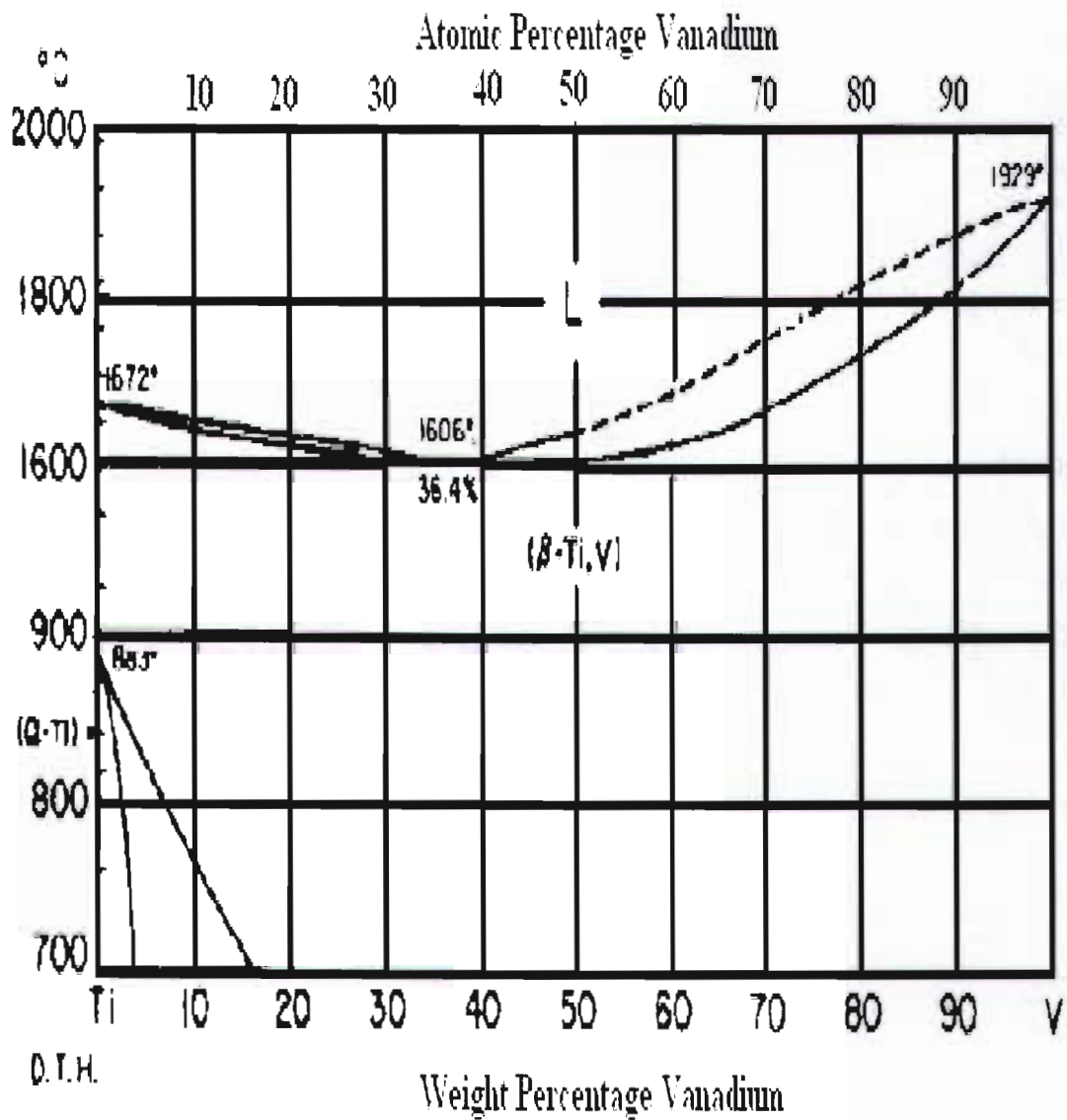


Figure 2.4: The Titanium Vanadium Phase Diagram (Smith, 1981: 56).

According to Clark & Varney, 1965: 447 and Askeland, 1996: 427-429; titanium (grade 5) alloy is an alpha-beta alloy containing two phases (Figure 2.5). A good annealing process can be used to improve its microstructure, and mechanical properties. A beta-stabilizing element is present in a high percentage in this alloy, and is responsible for a microstructure that is metastable beta, after solution annealing. At room temperature, a proper balancing of the alpha and beta stabilizers produces a mixture of alpha and beta phases (Smallman & Ngan, 2007: 342-343).

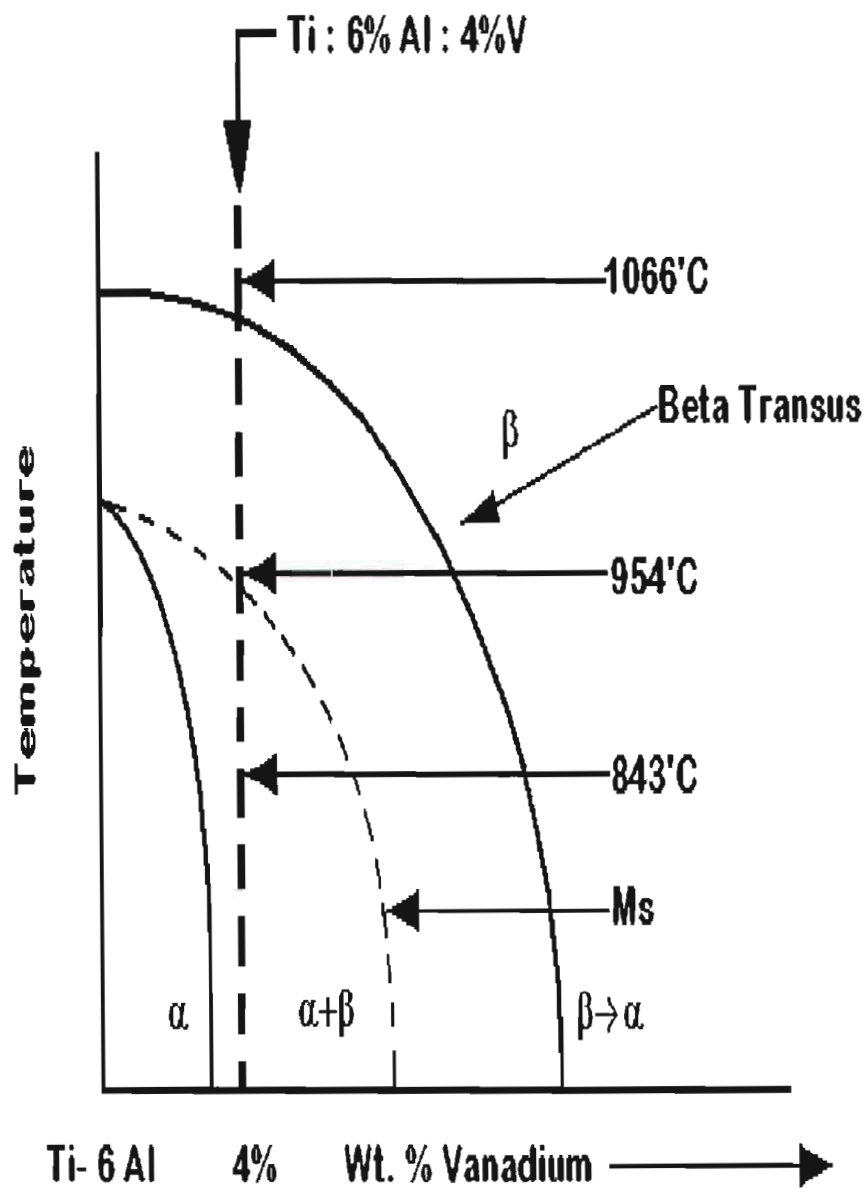


Figure 2.5: Pseudo-binary phase diagram of Ti6Al4V (Smith, 1981: 61).

When heated slightly below the beta transus temperature, a small amount of alpha is retained to prevent grain growth (the movement of grain boundaries by diffusion), and to reduce the amount of grain boundary area, thus causing small grains to ease off while those left become larger (Figure 2.5). With a proper cooling rate maintained, very good and uniform properties (high ductility, formability, good fracture toughness, high strength, low fatigue crack growth rate, and good resistance to creep) are achieved (Stoloff & Sikka, 1996: 299-310). Precipitation of alpha during ageing can be used to strengthen the alloy (Porter & Easterling, 1995: 115).

## 2.10 Factors considered in the welding of titanium

In the joining of materials, many factors of the processes of welding are considered. So in the welding of titanium, some factors of its welding processes have to be taken into consideration too. Such factors include costs, as shown in Table 2.6; the common commercial grades and alloys of titanium and their compositions (Table 2.7); as well as the design of the welded joints (Table 2.8). Other important factors to consider are, the composition of the electrode used in the welding processes (Table 2.9), the ease with which the different processes can be carried out (Table 2.10), the strength and durability of the welds, and the intended use(s) of the welded products.

**Table 2.6: Comparison of Welding processes based on Cost** (Donachie, 2000:209).

COST FACTOR	EBW	PAW	GTAW	GMAW
Equipment	Very high	Moderate	Low	High
Welding (Less equipment)	Low	Low	High	Moderate
Wire required	No	Sometimes	Often	Always
V groove required	No	No	Often	Always
Distortion	Very Low	Moderate	Very high	High

**Table 2.7: Nominal Chemical composition of common commercial titanium alloy grades (www.timet.com).**

ASTM Grade	N Max	C Max	H Max	Fe Max	O Max	Al	V	Ni	Mo	Nb	Cr	Zr	Pd	Residuals,	
														Ea Max	Total Max
<b>1</b>	0.0 3	0.0 8	0.015	0.2 0	0.1 8	—	—	—	—	—	—	—	—	0.1 0	0.40
<b>2</b>	0.0 3	0.0 8	0.015	0.3 0	0.2 5	—	—	—	—	—	—	—	—	0.1 0	0.40
<b>3</b>	0.0 5	0.0 8	0.015	0.3 0	0.3 5	—	—	—	—	—	—	—	—	0.1 0	0.40
<b>5</b>	0.0 5	0.0 8	0.015	0.4 0	0.2 0	5.5-6.75	3.5- 4.5	—	—	—	—	—	—	0.1 0	0.40
<b>7</b>	0.0 3	0.0 8	0.015	0.3 0	0.2 5	—	—	—	—	—	—	—	.12-. .25	0.1 0	0.40
<b>9</b>	0.0 3	0.0 8	0.015	0.2 5	0.1 5	2.5-3.5	2.0- 3.0	—	—	—	—	—	—	0.1 0	0.40
<b>11</b>	0.0 3	0.0 8	0.015	0.2 0	0.1 8	—	—	—	—	—	—	—	.12-. .25	0.1 0	0.40
<b>12</b>	0.0 3	0.0 8	0.015	0.3 0	0.2 5	—	—	.6-.9	.2-.4	—	—	—	—	0.1 0	0.40
<b>16</b>	0.0 3	0.0 8	0.015	0.3 0	0.2 5	—	—	—	—	—	—	—	.04-. .08	0.1 0	0.40
<b>17</b>	0.0 3	0.0 8	0.015	0.2 0	0.1 8	—	—	—	—	—	—	—	.04-. .08	0.1 0	0.40
<b>18</b>	0.0 3	0.0 8	0.015	0.2 5	0.1 5	2.5-3.5	2.0- 3.0	—	—	—	—	—	.04-. .08	0.1 0	0.40
<b>19</b>	0.0 3	0.0 5	0.020	0.3 0	0.1 2	3.0-4.0	7.5- 8.5	—	3.5- 4.5	—	5.5- 6.5	3.5- 4.5	—	0.1 5	0.40
<b>20</b>	0.0 3	0.0 5	0.020	0.3 0	0.1 2	3.0-4.0	7.5- 8.5	—	3.5- 4.5	—	5.5- 6.5	3.5- 4.5	.04-. .08	0.1 5	0.40
<b>21</b>	0.0 3	0.0 5	0.015	0.4 0	0.1 7	2.5-3.5	—	—	14.0- 16.0	2.2- 3.2	—	—	—	0.1 0	0.40
<b>23</b>	0.0 3	0.0 8	0.015	0.4 0	0.1 3	5.5-6.5	3.5- 4.5	—	—	—	—	—	—	0.1 0	0.40
	0.0 3	0.0 5	0.015	0.4 0	0.1 7	2.5-3.5	—	—	14.0- 16.0	2.2- 3.2	—	—	.04-. .08	0.1 0	0.40

The design, welding and fabrication of titanium (grade 5) alloy pipe joints are performed bearing in mind that welded products begin to show signs of failure at the weldments (Den Hartog, 1961: 41-63). Therefore, the composition of any electrode(s) used is such that its material properties are compatible with the material properties of the parent titanium alloy, and the fabrication is expertly done to avoid any weld defect(s). Since different fluids have different properties, the properties of the fluid that would be conducted through the welded pipes are taken into account as well.

**Table 2.8: Titanium welded joint design specification (www.timet.com).**

Type	Thickness Range inches	Weld passes	Electrode Type	Electrode Inches Diameter	Filler Wire Inches Diameter	Root Opening (R.O.)	Angle of Bevel (A)	Lead (L)
<i>square</i>	0.010-0.062	single	Tungsten <sup>1</sup>	1/16	None	0	—	—
<i>Butt</i>	0.031-0.125	Single or Double <sup>2</sup>	Tungsten <sup>1</sup>	1/16	None	0	—	—
	0.031-0.125	Single	Tungsten	1/16-1/8	1/22-1/16	0-0.10T <sup>3</sup>	—	—
<i>Single</i>	0.062-0.125	Single	Tungsten	1/16-3/32	1/16	0-0.10T	30°-60°	0.10-0.25T
<i>Vee</i>	0.125-0.250	First	Tungsten	1/16-3/32	None	0-0.10T	30°-60°	0.10-0.25T
		Second	Tungsten	1/16-3/32	1/16-3/32	—	—	—
	0.125-0.500	First	Tungsten	3/32-1/8	None	0-0.10T	30°-90°	0.10-0.25T
		Second	Consumable	1/16	—	—	—	—
	0.125-0.500	Single-Multiple	Consumable	1/16	—	0-0.10T	30°-90°	0.10-0.25T
<i>Double</i>	0.250-0.500	Double	Tungsten	1/16-3/32	1/16	0-0.10T	30°-90°	0.10-0.25T
<i>Vee</i>	0.250-0.750	Double	Consumable	1/16	—	0-0.10T	30°-90°	0.10-0.25T
	0.750-1.500	Double-Multiple	Consumable	1/16	—	0-0.10T	30°-90°	0.10-0.25T
<i>Single</i>	0.250-0.500	First	Tungsten	1/16-3/32	1/16	0-0.10T	15°-30°	0.10-0.25T
<i>U</i>		Second	Tungsten	1/16-3/32	1/16	—	—	—
	0.250-0.750	First	Tungsten	1/16	None	0-0.10T	15°-30°	0.10-0.25T
		Second	Consumable	1/16	—	—	—	—
	0.250-1.000	Multiple	Consumable	1/16	—	0-0.10T	15°-30°	0.10-0.25T
<i>Double</i>	0.750-1.500	Double-Multiple	Tungsten	1/16-3/32	1/16	0-0.10T	15°-30°	0.10-0.25T
<i>U</i>	0.750-1.500	Double-First	Tungsten	1/16	None	0-0.10T	15°-30°	0.10-0.25T
		Double-Multiple	Consumable	1/16	—	—	—	—
	0.750-2.000	Double-Multiple	Consumable	1/16	—	0-0.10T	15°-30°	0.10-0.25T
<i>Fillet</i>	0.031-0.125	Single or Double	Tungsten	1/16	None-1/16	0-0.10T	0°-45°	0-0.25T
	0.125-0.500	Single or double	Tungsten	1/16-3/32	1/16	0-0.10T	30°-45°	0.10-0.25T
	0.250-1.000	Single or Double	Consumable	1/16	—	0-0.10T	30°-45°	0.10-0.25T

<sup>1</sup>. Thoriated tungsten electrodes

<sup>2</sup>. Double Pass:1 pass each side

<sup>3</sup>. T: thickness of base material

**Table 2.9: Titanium welding electrode composition (AWS A5.16-70) (www.timet.com)**

Base Metal		Composition, Wt. Percent*								
AWS Wire Classification	(ASTM) grade	C	O	H	N	Al	V	Fe	Other	Ti
<i>ERTi-1</i>	(1)	0.03	0.10	0.005	0.012	—	—	0.10	—	Remainder
<i>ERTi-2</i>	(1)	0.05	0.10	0.008	0.020	—	—	0.20	—	Remainder
<i>ERTi-3</i>	(2)	0.05	0.10-0.15	0.008	0.020	—	—	0.20	—	Remainder
<i>ERTi-4</i>	(2)	0.05	0.15-0.25	0.008	0.020	—	—	0.30	—	Remainder
<i>ERTi-4</i>	(3)									
<i>ERTi-4</i>	(4)									
<i>ERTi-6Al-4V</i>	(5)	0.05	0.15	0.008	0.020	5.5-6.75	3.5-4.5	0.25	—	Remainder
<i>ERTi-6Al-4V-ELI**</i>	(5)	0.04	0.10	0.005	0.012	5.5-6.75	3.5-4.5	0.15	—	Remainder
<i>ERTi-0.2Pd</i>	(7)	0.05	0.15	0.008	0.020	—	—	0.20	Pd 0.12-0.25	Remainder
<i>ERTi-3Al-2.5V</i>	(9)	0.05	0.12	0.008	0.020	2.5-3.5	2.0-3.0	0.25	—	Remainder
<i>ERTi-3Al-2.5V-ELI**</i>	(9)	0.04	0.10	0.005	0.012	2.5-3.5	2.0-3.0	0.15	—	Remainder
<i>ERTi-0.2Pd</i>	(11)									
<i>ERTi-12</i>	(12)	0.03	0.25	0.008	0.020	—	—	0.30	Mo 0.2-0.4 Ni 0.6-0.9	Remainder
<i>ERTi-0.2Pd</i>	(16)									
<i>ERTi-0.2Pd</i>	(17)									

\* Analysis for interstitial content to be made after the welding rod or electrode has been reduced to its final diameter. Single values are maximum percentage.

\*\* This classification of filler metal restricts allowable interstitial content to a low level in order that the high toughness required for cryogenic applications and other special uses can be obtained in the deposited weld metal

**Table 2.10: Comparison of Welding processes based on the ease with which they can be performed** (Donachie, 2000:209).

<b>USABILITY CHARACTERISTICS</b>	<b>EBW</b>	<b>PAW</b>	<b>GTAW</b>	<b>GMAW</b>
Common thickness range (in)	Foil to 3	1/8 to 3/8	1/32 to 1/4	¼ to 3+
Ease of application	Fair to good	Good	Good	Fair
Ease of welding	Excellent	Good	Good	Difficult
Grooved joint required	No	No	Often	Always
Automatic or manual	Automatic	Both	Both	Automatic
Mechanical properties	Excellent	Good	Fair	Fair
Quality of joint	Excellent	Excellent	Good	Good-Fair

## **Chapter 3 Pipe Modelling and Simulation**

### **3.1 Introduction**

When pipes are joined together, they form a pipeline or a network of pipes. Welding is a reliable method of joining materials to form a whole piece of structure, and in some cases, a long network of facility. This is so, because it is not practical to manufacture even the smallest of equipments as a single piece of material without any joint. In laying any pipe network, the pipes that make the network have to be joined to work as a single continuous unit. So in the design of joined materials, it is necessary to ensure that the joined unit can deliver, in terms of strength and performance, as much as a whole single unit of such material(s) would have done, at the least. Hence models of products and processes are necessary to show the practical effectiveness of the intended design.

The Ti6Al4V pipe models used for this analysis were created using a general software package, Pro/ENGINEER Wildfire 5.0 - a modelling package used to create models of parts and assemblies during the engineering and design processes of new product development. It creates models with realistic appearances, and this allows for easy visualisation of the parts and assemblies being created. This package is value driven, using dimensions and parameters – any change(s) in dimension or/and parameter such as volume, mass, surface area, and centre of gravity; would be updated in the feature of that particular part or assembly, and automatically propagated through the rest of the features in the model, thereby updating the entire model. The package uses the finite element method to analyse materials of the models, allowing for the evaluation and optimization of the structural and even thermal performance of product designs in a real world environment. Its *mechanica* feature is a module that enables simulations to be performed on product designs, to determine whether the designs satisfy the intended requirements before they are built.

### **3.2 Properties of materials of the models**

Titanium grade 5 alloy – Ti6Al4V was used as the parent material for the pipes, and welds were autogenous gas tungsten arc welding with helium as inert gas. The default data/properties of titanium alloys in Pro/ENGINEER Wildfire 5.0 software package were updated to include such data as the Distortion Energy (von Mises), Tensile Yield Stress, Unified Material Law, Tensile Ultimate Stress (highlighted in Table 3.1), the material type – unalloyed or low alloyed, the type of surface finish, and the material's Failure Strength Reduction Factor (Becht, 2005: 46-48; Boyer *et al.*, 1994: 517-542 and [www.timet.com](http://www.timet.com)). An update was done on the default data/properties in the software, to reflect the mechanical properties of the sections of the parent material affected by the heat from welding and the heat affected zone; in accordance with what was obtained from literature, as highlighted on Tables 3.1 and 3.2

A lot of the material properties in the heat affected zone were different from those of the parent alloy. Such differences reflected in the highlighted values used for the Poisson ratio, Young Modulus, Co-efficient of Thermal Expansion in Table 3.2; Tensile Yield Stress, Tensile Ultimate Stress in Table 3.1, and the Failure Strength Reduction Factor, on pages 43 and 44. The updated physical/mechanical properties were done according to The Titanium Metals Corporation standards for TIMETAL 6-4 (Tables 3.1 and 3.2).

**Table 3.1: Tensile Properties for TIMETAL 6-4.** (Properties and Processing of TIMETAL 6-4, [www.timet.com](http://www.timet.com)).

Product (in)	Condition	Specification	Dir	Temperature °F(°C)	UTS ksi (MPa)	0.2%YS ksi (MPa)	Elongation %	Reduction in Area %
0.025 - 1.000	Annealed	ASTM B265	L & LT	68 (20)	130 (895)	120 (828)	10	-
≤3.00 RD or Thk	Annealed	ASTM B348	L	68 (20)	130 (895)	120 (828)	10	25
≤4.00 RD or Thk	Annealed	Mil-T- 9047G	All	68 (20)	130 (896)	120 (827)	10	25
> 4.00 - 6.00	Annealed	Mil-T- 9047G	All	68 (20)	130 (896)	120 (827)	10	20
< 0.500	STD	Mil-T- 9047G		68 (20)	165 (1137)	155 (1068)	10	20
> 0.500 - 1.000	STD	Mil-T- 9047G		68 (20)	160 (1103)	150 (1034)	10	20
> 1.000 - 1.500	STD	Mil-T- 9047G		68 (20)	155 (1068)	145 (999)	10	20
1.500 - 2.000	rd., sq., hex	Mil-T- 9047G		68 (20)	150 (1034)	140 (965)	10	20
2.000 - 3.000	rd., sq., hex	Mil-T- 9047G		68 (20)	140 (965)	130 (896)	10	20

**Table 3.2: Physical Properties for TIMETAL 6-4.** (Properties and Processing of TIMETAL 6-4, [www.timet.com](http://www.timet.com)).

Property	T(°F)	T(°C)	Value	Value (SI)
Density	72	22	0.160 lb in <sup>-3</sup>	4.42 g cm <sup>-3</sup>
Beta Transus	1825 ± 25	996 ± 14		
Melting (liquidus) point	3000-3020 ± 25	1650-1660 ± 14		
Thermal Conductivity	68	20	3.8Btu hr <sup>-1</sup> ft <sup>-1</sup> °F <sup>-1</sup>	6.6Wm <sup>-1</sup> K <sup>-1</sup>
	600	315	6.1Btu hr <sup>-1</sup> ft <sup>-1</sup> °F <sup>-1</sup>	10.6Wm <sup>-1</sup> K <sup>-1</sup>
Mil Annealed	1200	650	10.1Btu hr <sup>-1</sup> ft <sup>-1</sup> °F <sup>-1</sup>	17.5Wm <sup>-1</sup> K <sup>-1</sup>
Specific Heat	68	20	0.140Btu lb <sup>-1</sup> °F <sup>-1</sup>	0.580Jg <sup>-1</sup> K <sup>-1</sup>
	800	425	0.160Btu lb <sup>-1</sup> °F <sup>-1</sup>	0.670Jg <sup>-1</sup> K <sup>-1</sup>
	1600	870	0.220Btu lb <sup>-1</sup> °F <sup>-1</sup>	0.930Jg <sup>-1</sup> K <sup>-1</sup>
Magnetic Permeability			1.00005 at 20 oersteds	
Mean Coefficient of Thermal Expansion	32-212	0-100	5.0*10 <sup>-6</sup> in in <sup>-1</sup> °F <sup>-1</sup>	9.0*10 <sup>-6</sup> m m <sup>-1</sup> °C <sup>-1</sup>
	70-800	20-425	5.2*10 <sup>-6</sup> in in <sup>-1</sup> °F <sup>-1</sup>	9.4*10 <sup>-6</sup> m m <sup>-1</sup> °C <sup>-1</sup>
	70-1200	20-650	5.4*10 <sup>-6</sup> in in <sup>-1</sup> °F <sup>-1</sup>	9.7*10 <sup>-6</sup> m m <sup>-1</sup> °C <sup>-1</sup>
Electrical Resistivity	32	0	66 μΩin	1.68 μΩin
	600	315	73 μΩin	1.86 μΩin
	1200	650	74 μΩin	1.89 μΩin
Young Modulus	68	20	15.5-17.7 Msi	107-122 GPa
	450	230	13.8-16.2 Msi	
Shear Modulus	68	20	5.9-6.5 Msi	95-111 GPa
Poisson's Ratio	68	20	.31	.31

### 3.3 Dimensions of the Pipes

In this analysis, the dimensions and calibrations of the pipe models were adapted to those of The World Centre for Materials Joining Technology (The Welding Institute - TWI), Titanium Metals Corporation (TIMET), Titanium Information Group (TIG) and The American National Standards Institute (ANSI). In accordance with the above calibrations, the pipe model schedules were determined, using the ANSI pipe schedules (Table 3.3) as guide. They had an outer diameter of 8.625 inches (219.075 mm), and an inner diameter of 8.500 inches (206.375 mm).

**Table 3.3: ANSI pipe schedules, indicating wall thickness in inches.**

([http://www.vogeltool.com/pipe\\_schedules.html](http://www.vogeltool.com/pipe_schedules.html))

Pipe Size	OD	Schedule											
		5	10	20	30	40 (Standard)	60	80 (Extra Heavy)	100	120	140	160	2X Heavy
1/8	.405	.035	.049	-	-	.068	-	.095	-	-	-	-	-
1/4	.540	.049	.065	-	-	.088	-	.119	-	-	-	-	-
3/8	.675	.065	.065	-	-	.091	-	.126	-	-	-	-	-
1/2	.840	.065	.083	-	-	.109	-	.147	-	-	-	.187	.294
3/4	1.050	.065	.083	-	-	.113	-	.154	-	-	-	.218	.308
1	1.315	.065	.109	-	-	.133	-	.179	-	-	-	.250	.358
1-1/4	1.66	.065	.109	-	-	.140	-	.191	-	-	-	.250	.382
1-1/2	1.9	.065	.109	-	-	.145	-	.2	-	-	-	.281	.4
2	2.375	.065	.109	-	-	.154	-	.218	-	-	-	.343	.436
2-1/2	2.875	.083	.12	-	-	.203	-	.276	-	-	-	.375	.552
3	3.5	.083	.12	-	-	.216	-	.3	-	-	-	.437	.6
3-1/2	4	.083	.12	-	-	.226	-	.318	-	-	-	-	.636
4	4.5	.083	.12	-	-	.237	.281	.337	-	.437	-	.531	.674
4-1/2	5	-	-	-	-	.247	-	.355	-	-	-	-	.710
5	5.563	.109	.134	-	-	.258	-	.375	-	.500	-	.625	.75
6	6.625	.109	.134	-	-	.280	-	.432	-	.562	-	.718	.864
7	7.625	-	-	-	-	.301	-	.5	-	-	-	-	.875
8	8.625	.109	.148	.250	.277	.322	.406	.5	.593	.718	.812	.906	.875
9	9.625	-	-	-	-	.342	-	.5	-	-	-	-	-

There were different lengths of the pipes considered in this analysis. They ranged from 50 mm to 1500 mm long. This was done knowing that the lengths of pipes in industrial pipe networks, and all pipes in any given network can hardly be of equal length.

In order to have a closer focus and more precise analysis, the sections of the pipe network analysed were reduced to lengths between 50 mm and 100 mm, from between 1000 mm and 1500 mm. There were different lengths considered for the heat affected zones of the seam welded pipe models, to correspond with the different pipe lengths of the models. However, the width of the weldments and heat affected zones on every welded model remained the same in accordance with the analytical determination (Adams, 1958: 210). The simulation results of the reduced models also served to check and authenticate the results of the longer pipe models.

### 3.4 Pipe modelling

Using the *standard* mode in ProENGINEER Wildfire 5.0, sketches were drawn, dimensioned, extruded, and materials removed and/or added where necessary; to bring about each part of the desired models. Every part model (component of the assembled pipe models) was made in a separate window and later ‘exported’ to the assembly window. It was considered good practice to always check, and set the windows to the right units of measurement before sketching any model(s). Materials and their specific (materials’) properties were assigned to the different parts, while they remained individual parts. The different part models were then ‘exported’ to the *assembly* mode, where they were put together to become the designed pipe section/pipe network section models. Models of pipes with weldments at varying different positions along their lengths were created. However, as baseline markers (or control models), two unwelded pipe models of length 1000 mm and 50 mm were created (Figures 3.1 and 3.2). They are referred to in this thesis as unwelded models or control models. The pipe models with welded joints (on them) include the following:

- The pipe models with a single seam weldment along their length, parallel to the fluid flow direction (Figures 3.3 and 3.4) – the “seam weld” models of 1000 mm and 50 mm in length.
- A joined pipe model with a weld along the circumference, equidistant from both ends of the pipe model, and perpendicular to the fluid flow direction (Figures 3.5 and 3.6) – the “circumference weld” models of 1000 mm and 50 mm in length.

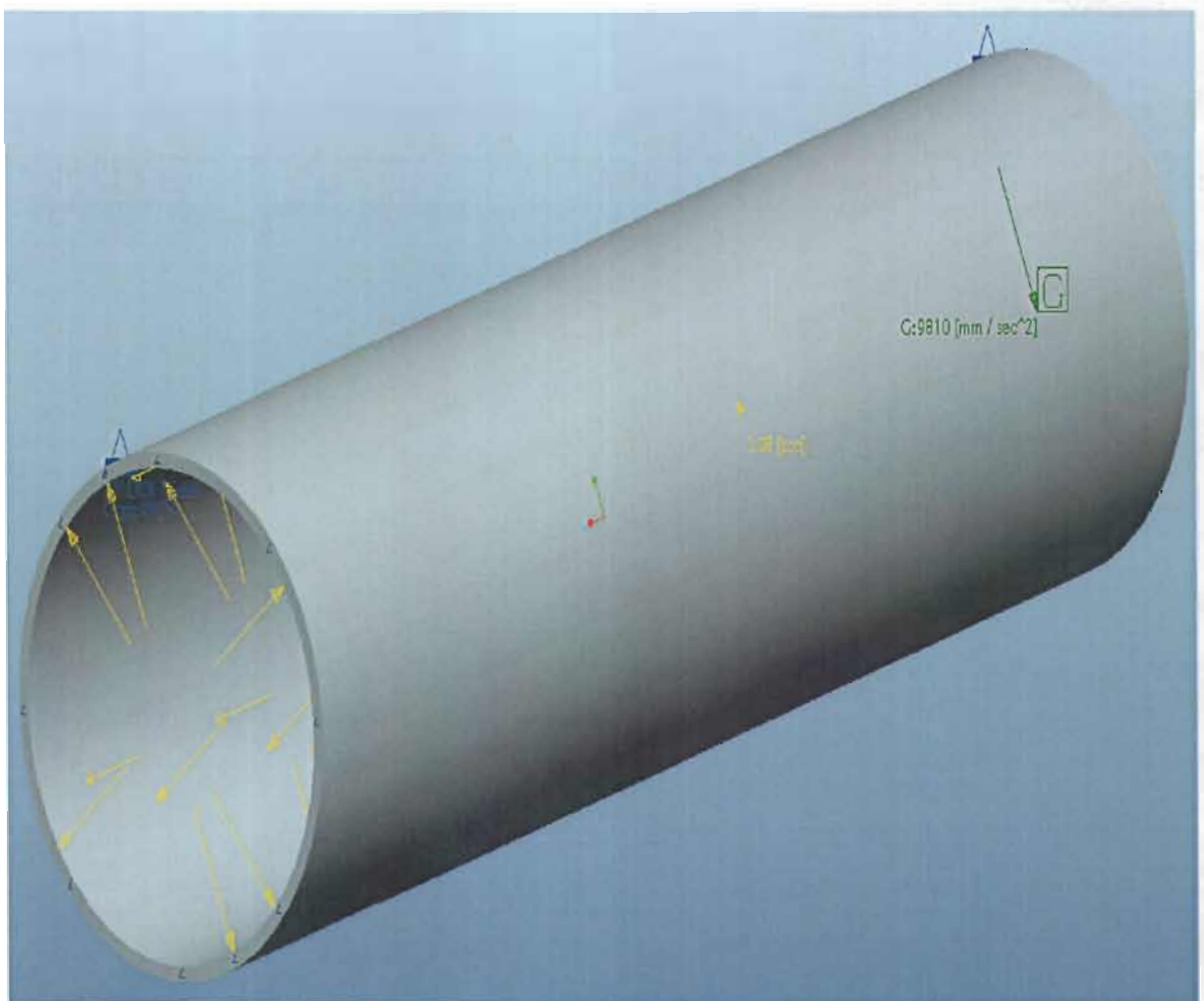


**Figure 3.1: Unwelded pipe (Control) model of 1000 mm length showing constraints and load (gravity, flow and pressure).**

The different part models of the assembled models were assigned different colours for easy identification. As shown in Figures 3.2, 3.4, and 3.6, a reduced version of each of

the models was created, to allow for more detailed analysis, as explained later in this chapter. The windows of the fully assembled models were then switched to the *mechanica* mode, where the geometrical co-ordinates, constraints, pressures, forces and fluid flow loads were incorporated into the analysis. After setting the plotting grid, polynomial order, percentage convergence, the combined constrained sets, and summed load sets; towards achieving the intended aim of each set of analyses, the simulations were made to run, and were monitored on the *display study status* window. Some results of interest, of some of the models analysed are presented in Tables 4.1 and 4.2. And in

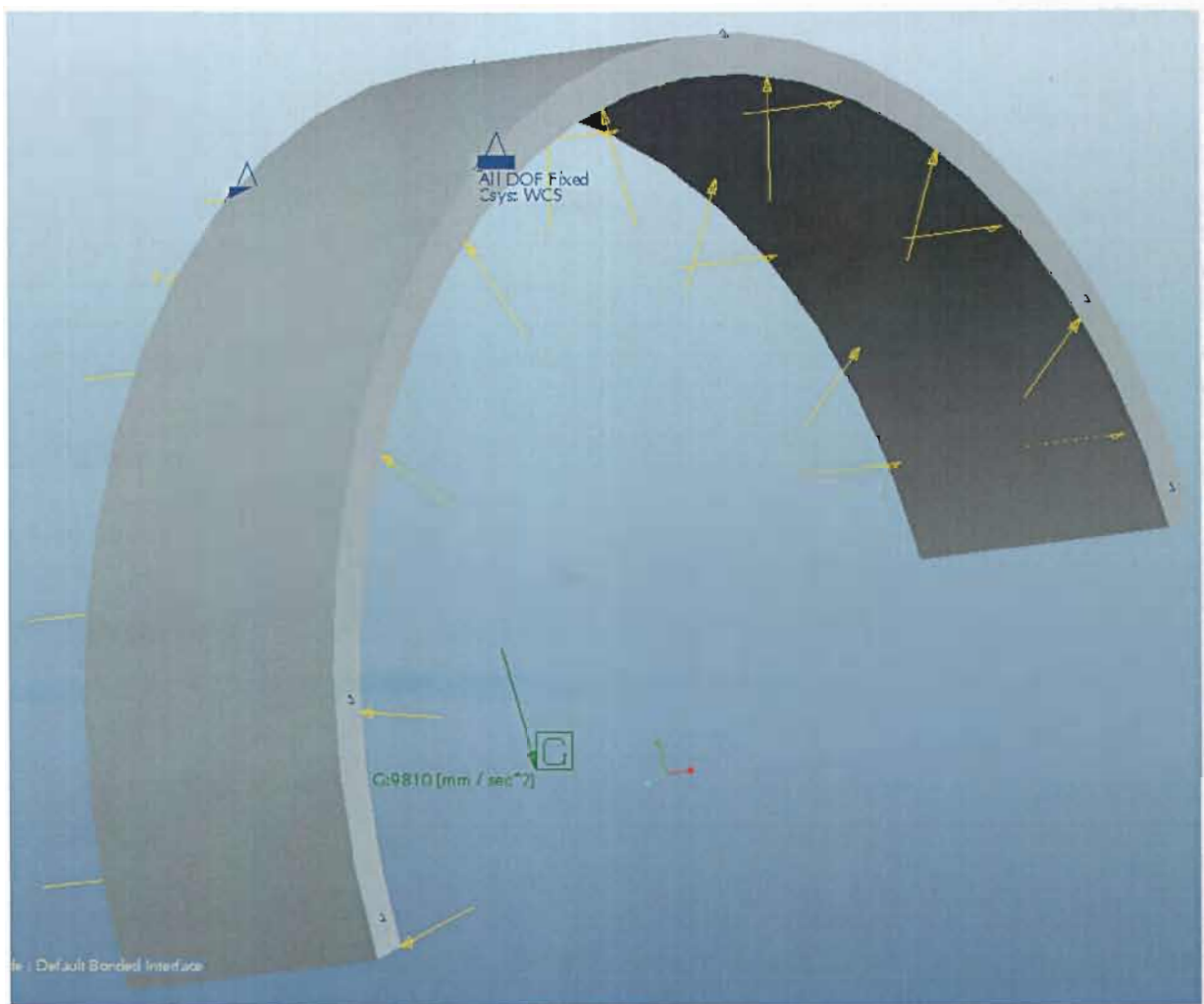


**Figure 3.2: Unwelded pipe (Control) model of 50 mm length showing constraints and load (gravity, flow and pressure).**

the appendices are samples of the simulation process data for the analysed models. Among other information contained in the appendices (A to D), the models' number of elements, number of points, edges and faces are recorded. The maximum displacements along each of the coordinates – abscissa, ordinate and applicate are also shown in the appendices.



**Figure 3.3:** “Seam-weld” pipe (SWP) model of 1000 mm length showing constraints and load (gravity, flow and pressure).

Besides the ease of identification, the different part models of each assembled model were assigned different colours to aid visual observation while assembling the parts, in incorporating the geometrical co-ordinates, constraints, pressures, forces and fluid flow loads; and during the simulation analyses. The geometrical co-ordinate used was the global geometrical co-ordinates, and the pipe models were constrained from rotational and translational motions but free to experience radial motion. There were fluid flow and internal pressure loaded evenly on all points on the inner walls of the models. There was gravitational force loaded too.

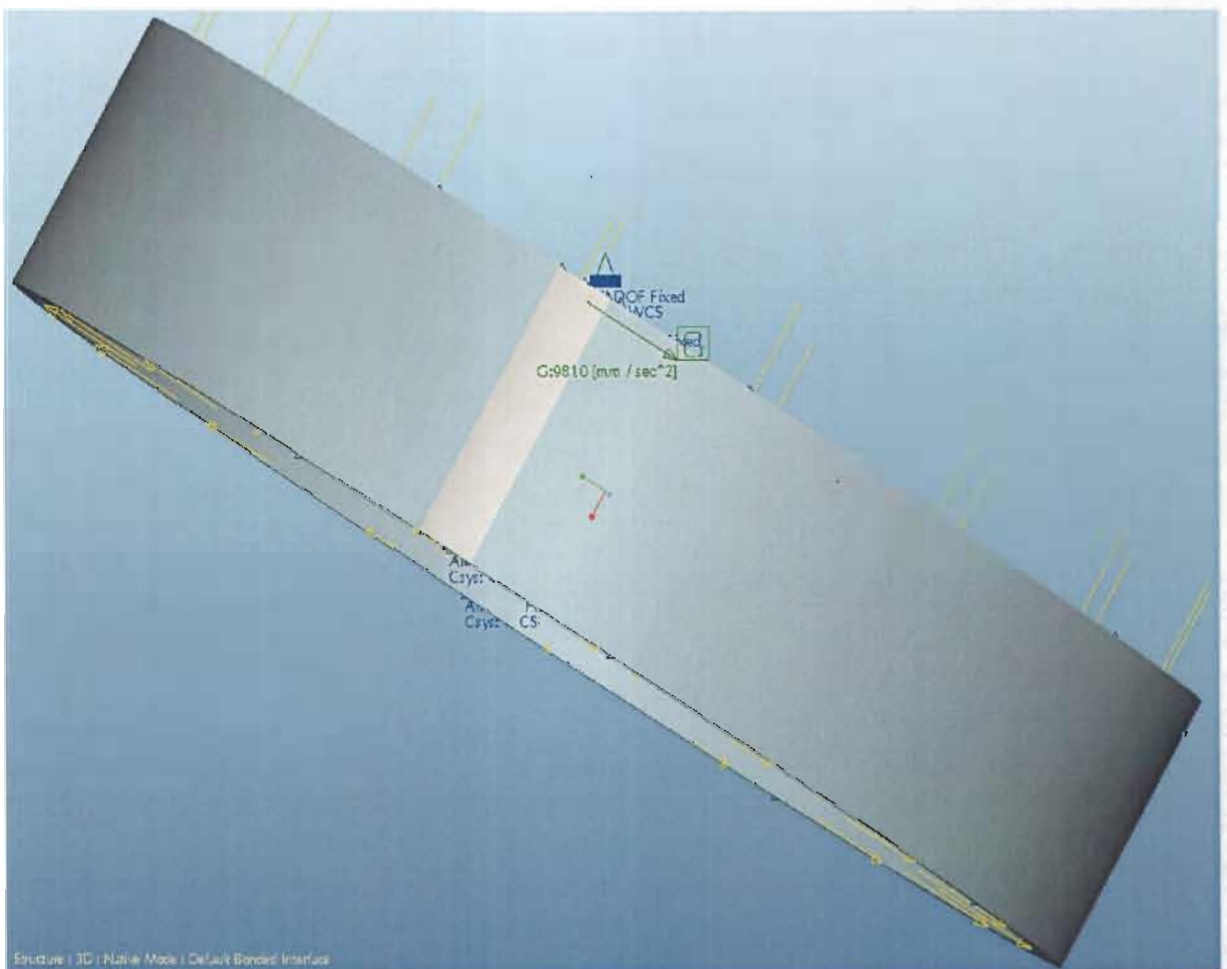


**Figure 3.4: “Seam weld” pipe (SWP) model of 50 mm length showing constraints and load (gravity, flow and pressure).**

The different welding positions were chosen so as to observe the difference(s) in welding at different sections along the pipe network, if there were any. As a result of the welded joints being modelled at varying different positions, different components of the different models differed in length, though they had the same wall thickness. However, the width of the heat affected zones of the welded pipe models remained the same.

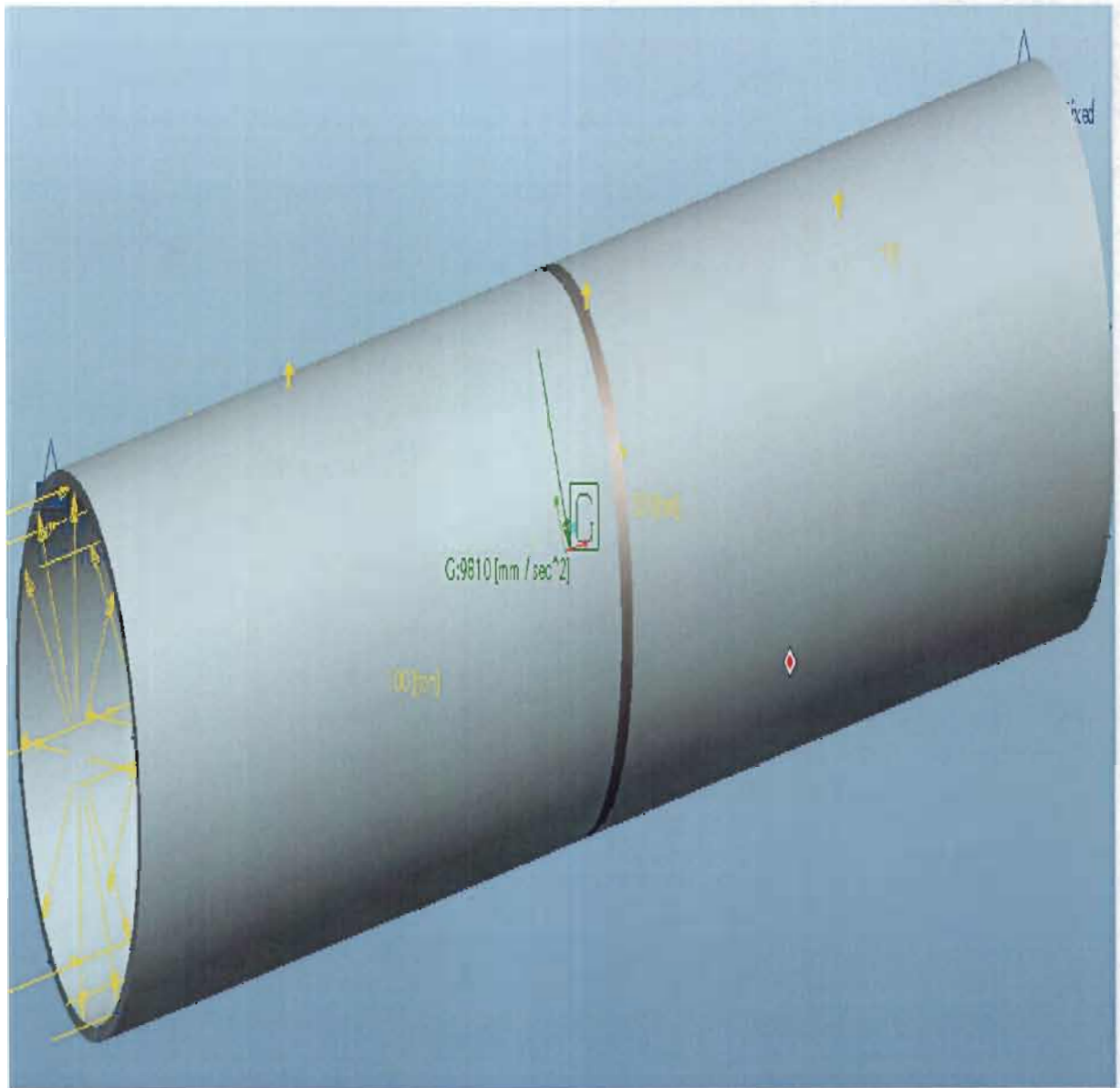


**Figure 3.5:** “Circumference weld” (CW) pipe model of 1000 mm length constraints and load (gravity, flow and pressure).

Pipes do not have width. Hence the parameters presented in Table 3.4 for the pipe models' parent alloy components and unwelded pipe models give their lengths as well as

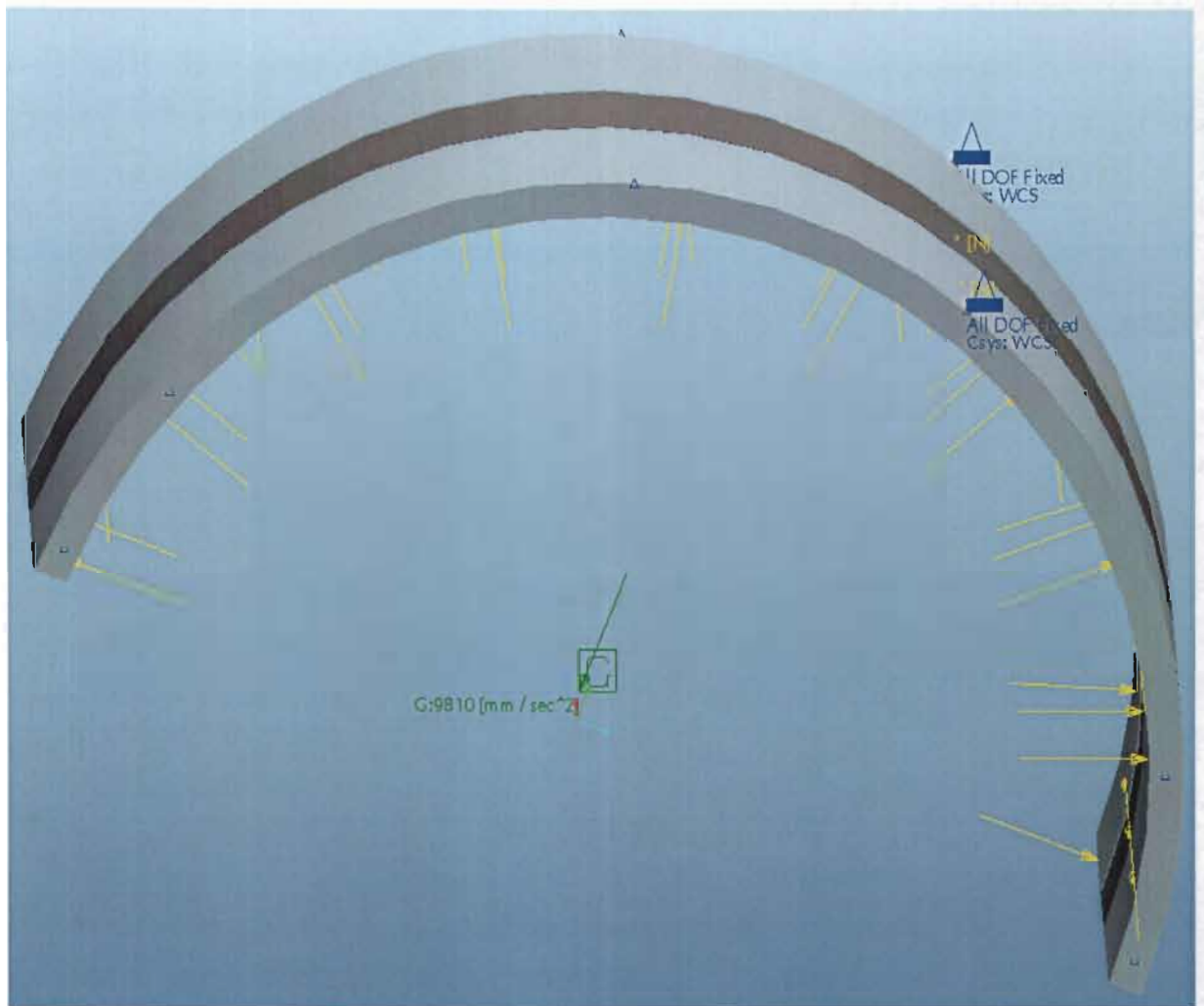


**Figure 3.6:** “Circumference weld” (CW) pipe model of 50 mm length showing constraints and load (gravity, flow and pressure).

their inner and outer diameters (wall thickness) only. Nevertheless, the welded pipe models had parameters for the width of the heat affected zones, but no parameters for lengths, in accordance with welding practice. The two unwelded pipe (control) models were not welded at any point, so they had no parameters for the width of the heat affected

zones. None of the components of the ‘seam weld’ pipe models had a circumference, hence they had no diameters. The dimensions of the models are presented in Table 3.4.

**Table 3.4: Dimensions of models (and their component parts)**

Model	Component	Length (mm)	Diameter (mm)		Width (mm)
			Inner	Outer	
Unwelded	Parent alloy	1000	206.375	219.075	N/A
Unwelded (reduced)	Parent alloy	50	206.375	219.075	N/A
Seam welded pipe	Parent alloy	1000	N/A	N/A	N/A
	Heat affected zone	1000	N/A	N/A	12
Seam welded pipe (reduced)	Parent alloy	50	N/A	N/A	N/A
	Heat affected zone	50	N/A	N/A	12
Pipe welded along its circumference	Parent alloy	494	206.375	219.075	N/A
	Heat affected zone	N/A	206.375	219.075	12
Pipe welded along its circumference (reduced)	Parent alloy	19	206.375	219.075	N/A
	Heat affected zone	N/A	206.375	219.075	12

\*N/A: Not applicable

In developing the welded pipe models, different flow rate values were used for the fluid flowing through the pipes. Flow rates are commonly measured in barrels per day in major sectors like the oil and gas industry. Since the software used for the analysis does not accommodate fluid in volumes, and measurements in million barrels per day (mbpd), the common industry units of measurement of volume flow rates were converted from million barrels per day (mbpd) to cubic meters per second ( $\text{m}^3/\text{s}$ ). And using the relationship:

$$m = \rho Q$$

where

3.1

$m$  = mass flow rate of the fluid

$\rho$  = density of the fluid

$Q$  = volume flow rate of the fluid;

the volume flow rates [in cubic meters per second ( $\text{m}^3/\text{s}$ )] were converted to mass flow rates (in kilograms per second), and then to (tonnes per second).

Typical values for mass flow rates commonly used in industry are not freely available because of industry privacy policies and sector competition. However, information was acquired by private communication with two sources in two firms. From the information, values for the mass flow rates of the fluid ranged from 155.86 tonnes/second (100,000 bpd) to as much as 187.03 tonnes/second (1mbpd). For the same reason advanced for converting the units of measurement of volume in industry to the one used in this analysis, the common units of measurements of pressure in the oil and gas sector – pounds/square.inch (psi) and bar were converted to mega Pascal (MPa). Hence internal pressure values of between 28 MPa and 40 MPa on the internal walls of the pipes were used for the simulation. In accordance with the Bernoulli's equation:

$$\frac{p_1}{\rho g} + \frac{u_1^2}{2g} + z_1 = \frac{p_2}{\rho g} + \frac{u_2^2}{2g} + z_2, \quad 3.2$$

where

$p_1$  = pressure at point 1

$p_2$  = pressure at point 2

$u_1$  = fluid flow velocity at point 1

$u_2$  = fluid flow velocity at point 2

$\rho$  = density of the fluid at all points

$g$  = acceleration due to gravity

$z$  = elevation;

it was assumed that:

- The flow is steady.
- The density is constant (which also means the fluid is incompressible).

- The friction losses are negligible.

The equation relates the states of flow at two points, and in effect, the states of flow at all points within the analysed section of the pipe.

To reflect real life scenarios, the pipes were constrained in all rotational directions because when fluid is passing through pipes, the pipes do not rotate. Also, pipes do not experience translational movements while conducting fluid, so they were also constrained against any such (translational) movements. However, they were unrestrained in the radial direction.

In order to have a more detailed analysis, for each and every model measuring between 1000mm and 1500mm long, there was a corresponding reduced model. This was done to increase the number of finite elements per unit area of the model of the small section of the pipe, since meshing the model of an independent small section of a pipe allows for the creation of finer elements, compared to the number of elements it (that small section) had when it was part of the full model. Therefore, the reduced model would give finer elements; even though it would have a considerably reduced number of (finite) elements as a detached whole model, in comparison to the original full model. All the reduced models of the analysed pipe models were of the same length - 50mm (Figures 3.2, 3.4 and 3.6). The length of the “parent” components of the reduced circumference welded pipe model was 19mm long, to accommodate the width of the heat affected zone (Figure 3.6).

To be able to accurately analyze the effect of the forces/pressure on the different parts/sections of the pipes, a symmetry constraint was used on the reduced models. The symmetry constraint allows half the section of the pipe models, perpendicular to the direction of fluid flow to be concealed. Thus, the pipe models appeared to have been sharply cut symmetrically, with one half showing and the other half seemingly removed (Figures 3.2, and 3.6). Also, this allowed the cross section of the thickness of the pipe walls to be viewed. So measurements of the simulated load effects on the cross-section of

the pipe walls could be taken. This made it possible to observe and analyze more detailed welding and load effect/s on the pipe models. The simulation results of the reduced pipe models were used as checks, by comparing them with those of the pipe models ranging from 1000 mm to 1500 mm.

## **Chapter 4 Finite Element Analysis Results and Discussion**

### **4.1 Introduction**

Simulations of the stresses on the pipe models were carried out using the Finite Element Method. There were many stress results recorded during the simulation, but the von Mises stress was of utmost interest since it determines whether the combination of the three principal stresses acting along the abscissa, ordinate and applicate axes at any given point along the pipe models will cause failure. The focus therefore, was on the von Mises stresses shown on the different sections of the loaded models. Some results of the simulation analyses are recorded in this chapter. The percentage deviations of the simulated results from the calculated hoop stress value are presented in this chapter as well. The different stress distributions and the difference in stress levels shown on different sections of the pipe models are discussed too.

### **4.2 FEM Results**

Some of the von Mises stress results shown on the loaded pipe models during simulation are given in Table 4.1. They are listed in terms of the minima and maxima values recorded on different sections of the different pipe models.

**Table 4.1: FEM Results**

Pipe models	Stress ( $10^2 \text{ N/mm}^2$ )	
	Minimum	Maximum
Unwelded	0.02	3.18
Unwelded (reduced)	0.06	3.17
Seam-welded	0.04	3.18
Seam-welded (reduced)	0.03	3.21
Circumference weld	0.02	3.19
Circumference weld (reduced)	0.06	3.20

The “fringe” displays of the simulated loaded models [Figures 4.1 (a) to 4.3 (b)] show the stress distributions on the models. They have a legend that indicates the magnitude of stress shown on different sections of the pipe models. The deep blue colour indicates minimum stress, and the stress level increases to its maximum, indicated in red.

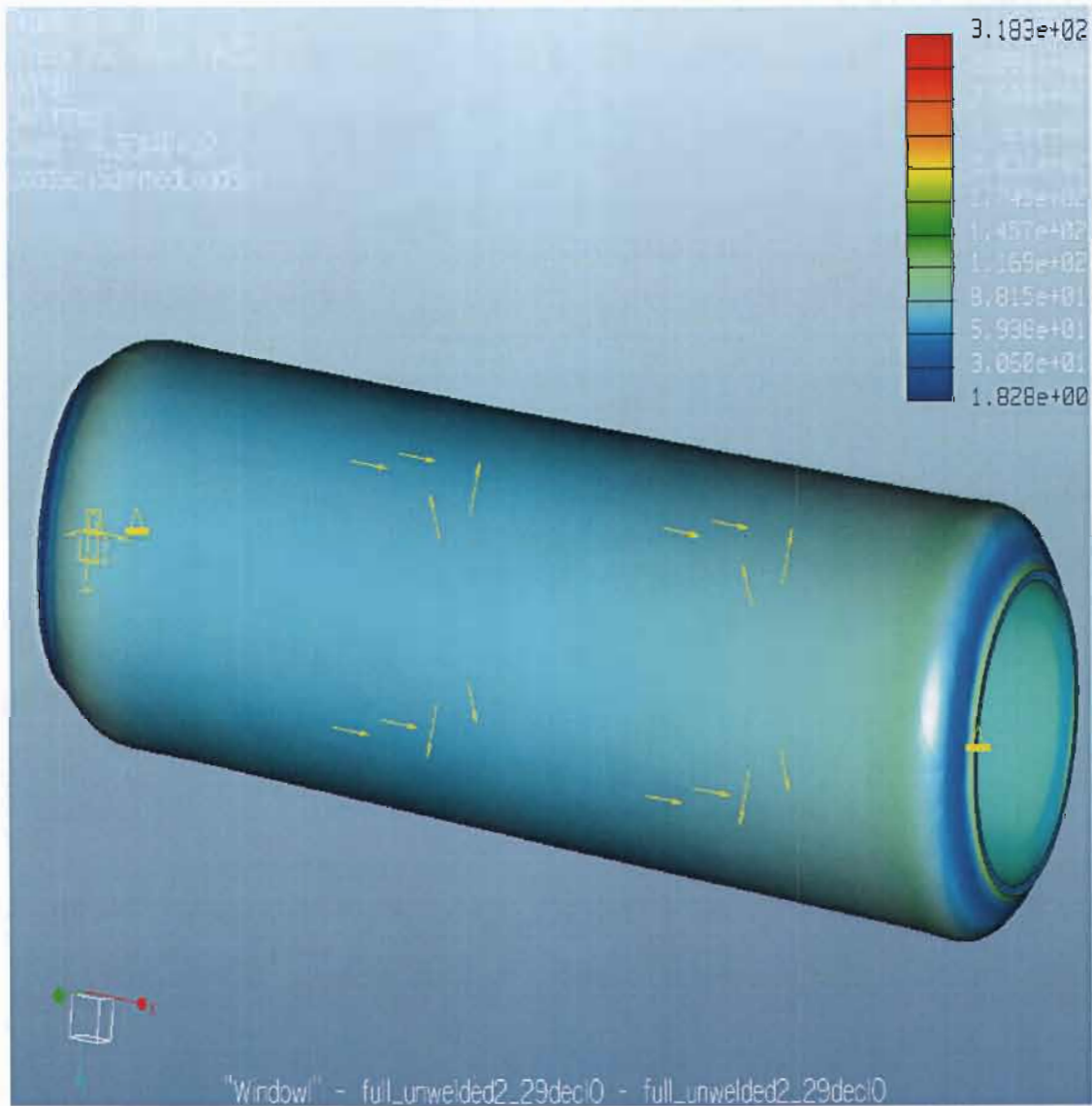


**Figure 4.1a: Stress distribution along the 1000 mm (unwelded) pipe model.**

The 1000 mm unwelded (control) pipe model had a minimum von Mises stress of  $1.828 \times 10^0$  N/mm<sup>2</sup> (approximately  $0.02 \times 10^2$  N/mm<sup>2</sup>) and a maximum von Mises stress of  $3.183 \times 10^2$  N/mm<sup>2</sup>.

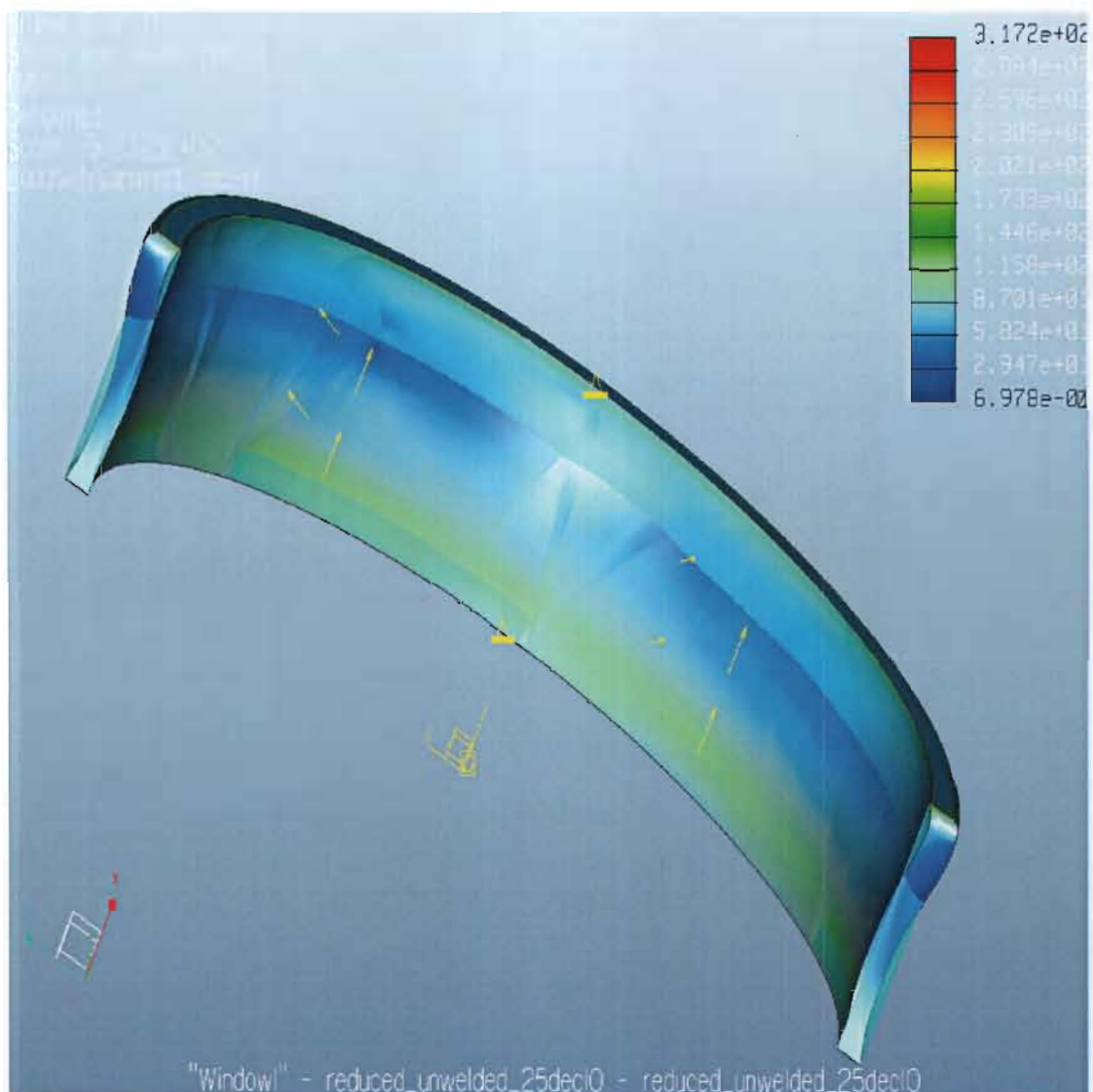


**Figure 4.1b: Stress distribution along the 50 mm (unwelded) pipe model.**

The 50 mm unwelded (control) pipe model had a minimum von Mises stress of  $6.978 \times 10^0$  N/mm $^2$  (approximately  $0.06 \times 10^2$  N/mm $^2$ ) and a maximum von Mises stress of  $3.172 \times 10^2$  N/mm $^2$ .

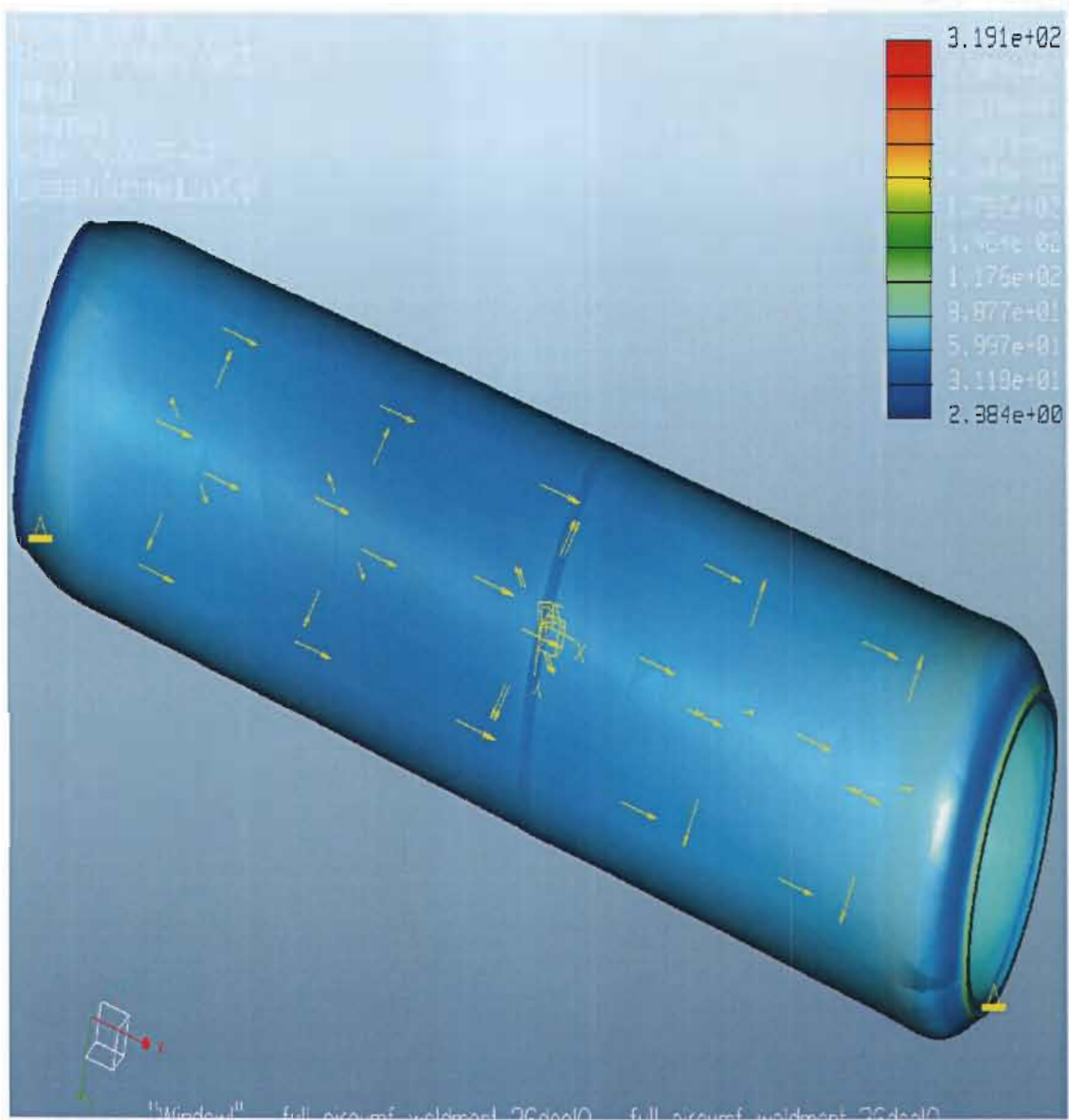


**Figure 4.2a:** Stress distribution along the 1000 mm “circumference weld” (CW) pipe model.

The 1000 mm pipe model welded along the circumference had a minimum von Mises stress of  $2.384 \times 10^2$  N/mm<sup>2</sup> (approximately  $0.02 \times 10^2$  N/mm<sup>2</sup>) and a maximum von Mises stress of  $3.191 \times 10^2$  N/mm<sup>2</sup>.

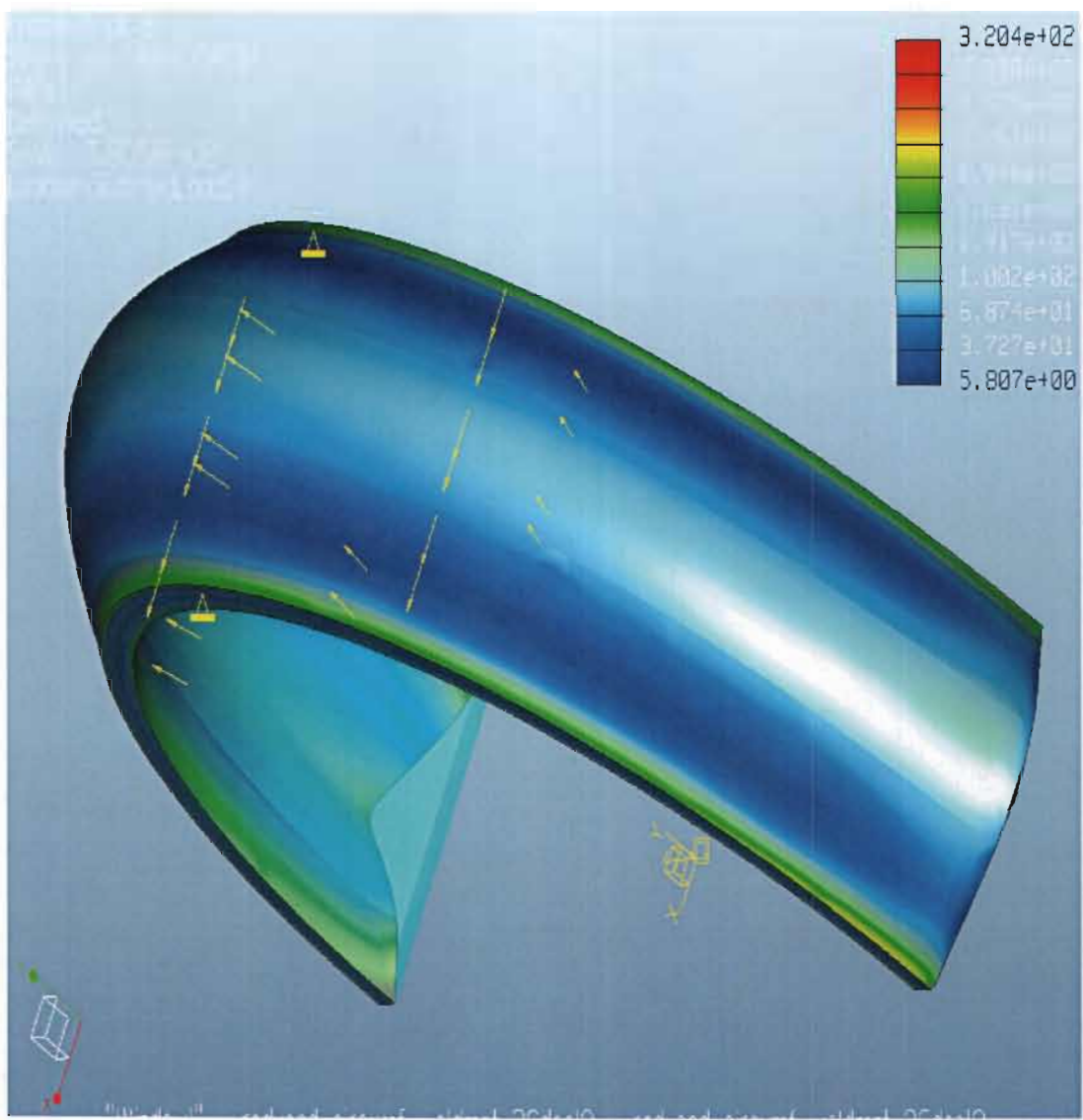


**Figure 4.2b: Stress distribution along the 50 mm “circumference weld” (CW) pipe model.**

The 50 mm pipe model welded along the circumference had a minimum von Mises stress of  $5.807 \times 10^0$  N/mm<sup>2</sup> (approximately  $0.06 \times 10^2$  N/mm<sup>2</sup>) and a maximum von Mises stress of  $3.204 \times 10^2$  N/mm<sup>2</sup>.

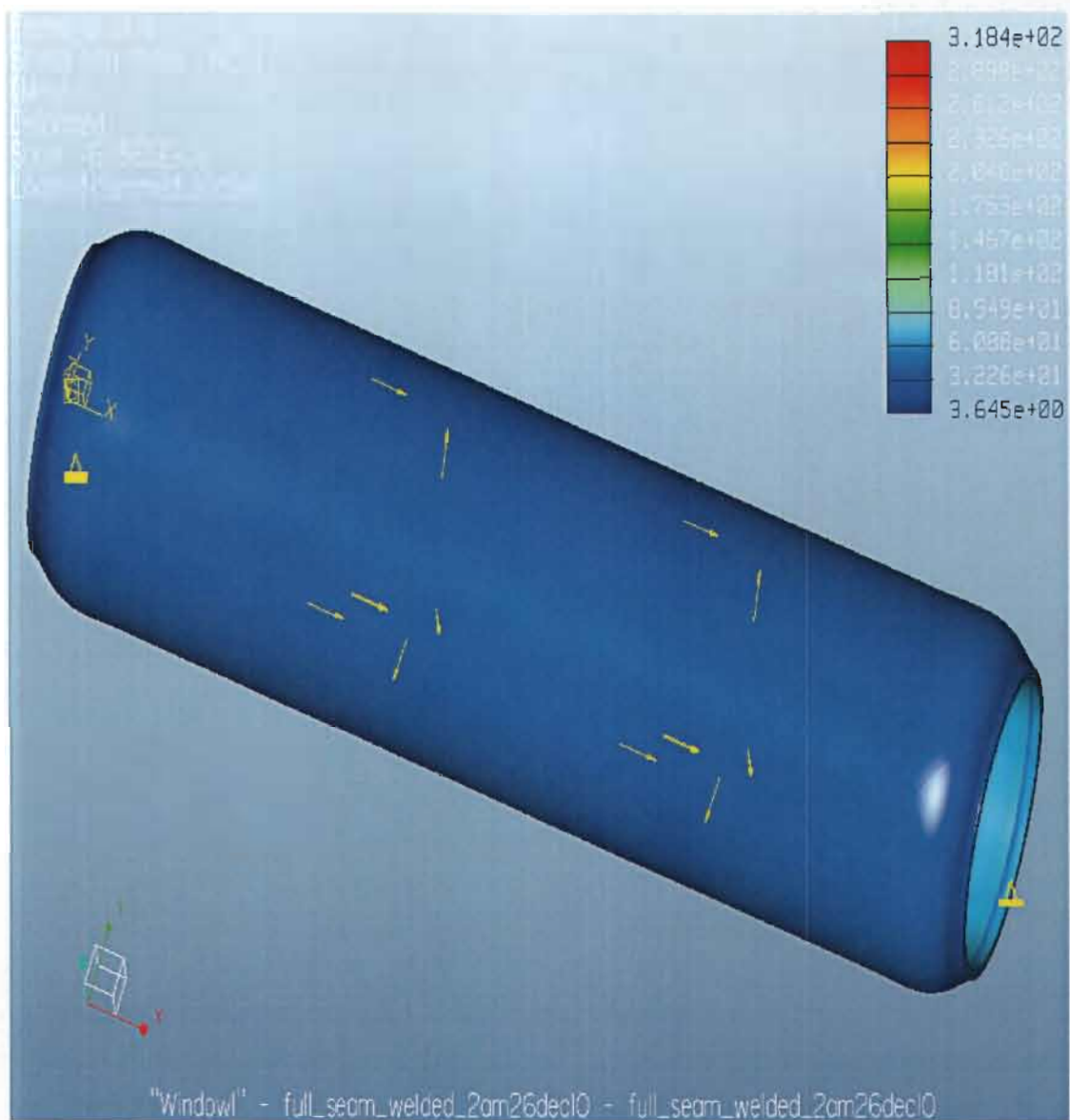


**Figure 4.3a: Stress distribution along the 1000 mm “seam weld” (SWP) pipe model.**

The 1000 mm pipe model welded along the seam had a minimum von Mises stress of  $3.645 \times 10^0$  N/mm<sup>2</sup> (approximately  $0.04 \times 10^2$  N/mm<sup>2</sup>) and a maximum von Mises stress of  $3.184 \times 10^2$  N/mm<sup>2</sup>.

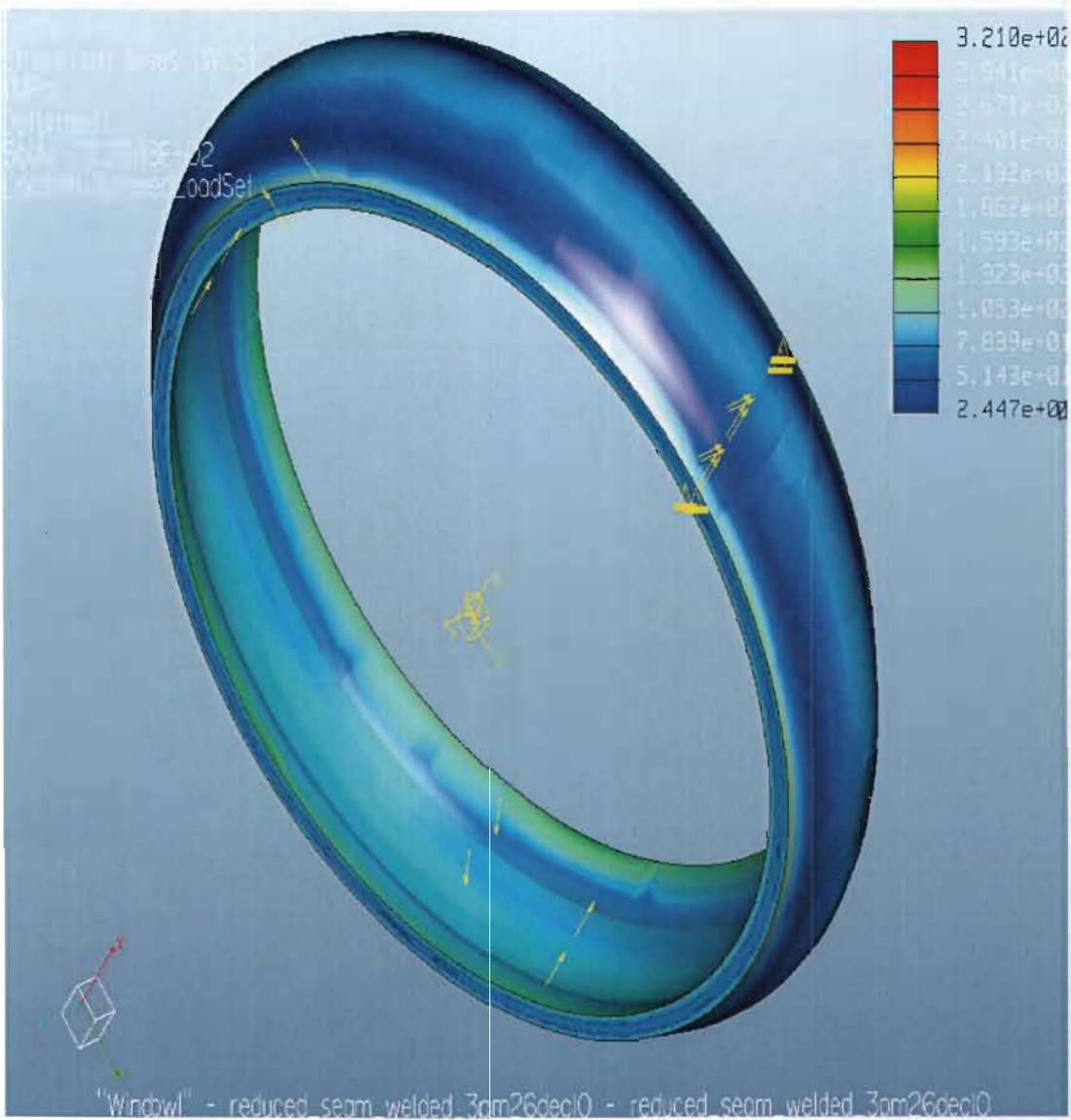


**Figure 4.3b: Stress distribution along the 50 mm “seam weld” (SWP) pipe model.**

The 50 mm pipe model welded along the seam had a minimum von Mises stress of  $2.447 \times 10^2$  N/mm $^2$  (approximately  $0.03 \times 10^2$  N/mm $^2$ ) and a maximum von Mises stress of  $3.210 \times 10^2$  N/mm $^2$ .

On the average, each round of the simulations recorded as many as twelve von Mises stress values for each of the pipe models. Nevertheless, it is only the maximum value that is of utmost interest in this research work. Of the twelve von Mises stress values recorded

for the unwelded pipe models [Figures 4.1 (a) and 4.1 (b)], for instance, the focus was on the highest of the values [ $3.183 \times 10^2$  N/mm<sup>2</sup> (on the full unwelded pipe model) and  $3.172 \times 10^2$  N/mm<sup>2</sup> (on the reduced unwelded pipe model)]; since they indicate the highest possible stresses the load can cause along the pipe models, and so was the focus on all other models. The ability or inability of the pipe models to withstand such high stress would indicate whether titanium alloy (grade 5) would be fit or unfit for use as material to make pipes that can conduct such fluid load.

### 4.3 Discussion of FEM Results

As observed in the simulation, and in agreement with literature (Becht, 2004: 29-35), the circumferential stress along the inner walls of the pipe models was higher than the circumferential stress shown on the outer walls. The legend on the fringe displays of the simulated pipe models [Figures 4.1 (a) to 4.3 (b)] served as guide in observing the stress distribution. The stress on the inner pipe walls was higher because of the fluid-structure interaction between the flowing fluid and the inner walls, and the effect of the internal pressure of the flowing fluid, which impacts directly on the inner walls (Lee *et al.*, 1995: 297-311; Niordson, 1953: 1-28 and Chen & Zhang, 1998: 38-45). The distribution of stress along the thickness of the pipe walls is more visibly illustrated on the reduced and symmetrically constrained pipe models in this work [Figures 4.1 (b) and 4.2 (b)]. The least minimum von Mises stress of approximately  $0.02 \times 10^2$  N/mm<sup>2</sup> (on two of the analysed pipe models) and the highest maximum von Mises stress of  $3.21 \times 10^2$  N/mm<sup>2</sup> (on the reduced seam welded pipe model) were recorded.

In pipe design and analysis, according to the ASME B31.3 code (Becht, 2004: 20-21), stress is analytically calculated as a function of location through the wall thickness of pipes using the equation:

$$\sigma_h = P \frac{0.5(D/t)^2 - (D/t) + 1}{(D/t) - 1} \quad 4.1$$

where

$$\sigma_h = \text{hoop stress}$$

$P$  = internal (design) pressure

$D$  = outside diameter of the pipe

$t$  = pressure design thickness

In this analysis, equation 4.1 was used to verify the simulated maximum von Mises stresses that the pipe models experience when put under load that is within the practical range of interests. So substituting the dimensions and parameters of the pipe models into the above equation, the calculated hoop stress is:

$$\begin{aligned}\sigma_h &= 40 \left[ \frac{0.5(219.075/12.7)^2 - (219.075/12.7) + 1}{(219.075/12.7) - 1} \right] \\ &= 321.308 \text{ N/mm}^2 \\ &\approx 3.21 \times 10^2 \text{ N/mm}^2\end{aligned}$$

The simulated maximum von Mises stress results are verified using the analytically determined hoop stress value by comparing it with the simulated values. And the closeness of the simulated results of the maximum von Mises stress shown on the analysed pipe models to the calculated hoop stress value is determined by the percentage deviation of the experimental results from the analytical value. The percentage deviation is calculated using the formula:

$$\frac{\sigma_{hD} - \sigma_{hF}}{\sigma_{hD}} \% \quad 4.2$$

where

$\sigma_{hD}$  = analytical (calculated) hoop stress

$\sigma_{hF}$  = simulated von Mises stress

The simulated maximum von Mises stress of the reduced model of the seam welded pipe ( $3.21 \times 10^2 \text{ N/mm}^2$ ) is the same as the calculated hoop stress value, giving a 0.00% deviation from the calculated value, while the simulated maximum von Mises stress of the reduced model of the unwelded pipe ( $3.172 \times 10^2 \text{ N/mm}^2$ ) has the highest deviation of 1.25% from the calculated hoop stress value. The percentage deviations of the simulated maximum von Mises stress results of the different pipe models from the analytical hoop

stress value of  $3.21 \times 10^2$  N/mm<sup>2</sup> (obtained from equation 4.1) are presented in Table 4.2 below.

**Table 4.2: Percentage deviation of simulated maximum von Mises stress results from the calculated hoop stress value ( $\sigma_{hD} = 3.21 \times 10^2$  N/mm<sup>2</sup>).**

Pipe models	von Mises Stress ( $\sigma_{hF}$ ) ( $10^2$ N/mm <sup>2</sup> )	Percentage deviation (%)
Unwelded	3.18	0.94 (lower)
Unwelded (reduced)	3.17	1.25 (lower)
Seam-welded	3.18	0.94 (lower)
Seam-welded (reduced)	3.21	0.00
Circumference weld	3.19	0.62 (lower)
Circumference weld (reduced)	3.20	0.31 (lower)

Generally, all the reduced models showed von Mises stress values that were very close to those shown by their corresponding full models. And all the simulated pipe models recorded von Mises stress values that were very close to the calculated hoop stress value. In terms of the stress distribution, the results of the legend displays of the reduced models were in agreement with those of their corresponding full models. The welded models, too, showed numerical results that are very close to those of the unwelded (control) models. The different models, welded at different positions, are discussed in sections 4.3.1 through 4.3.3.

#### 4.3.1 The Unwelded (control) Pipe Models

Stress was shown to be highest at both ends of the unwelded pipe models. In this case, the points on the pipeline that were rigidly supported against gravity and flexural movement were represented by the pipe models' ends. At the supported points, the fluid effectively developed a very slight flow constriction as a result of the rigid support, thereby having more impact on the walls of the pipe models (Lee *et al.*, 1995: 297-311

and Païdoussis, 1998: 88-104). Stress was shown to be least at two small sections – one being adjacent to the inflow end of the pipe models and the other adjacent to the outflow end. Minimal stress was shown at the small section close to the inflow end because the fluid momentarily lost impetus after constriction at the supported point, before it continued in the flow direction. Similarly, at the outflow end, the fluid momentarily lost impetus before being constricted at the supported point. Figures 4.1 (a) and 4.1 (b) on pages 58 and 59 show that stress increased slightly and then remained unchanged through the section of the pipe models' lengths, between the two least stressed small sections, largely due to the steady state of flow along the section and the fact that the fluid had been confined to the constant flow boundaries of the pipe model for a considerably long stretch. With the width of the pipe models being consistently the same through its length, and even (smooth) inner walls along the entire pipe length, the flow boundary remained unchanged; enhancing a steady state of flow along the section not affected by flow constriction. Though the models represent a very short section in the middle of a pipeline, it showed that in reality, the changes in flow constriction at the supported points of a pipe network impact on the fluid flow behaviour (e.g. Niordson, 1953: 1-28; Freitas Rachid & Costa Mattos, 1998: 139-160 and Chen & Zhang, 1998: 38-45). It is worth noting that the difference in the maxima stress magnitudes of the two unwelded pipe models (the 1000 mm model and the reduced 50 mm model) are negligibly small ( $0.01 \text{ N/mm}^2$ ), and could only be detected by very sensitive tools such as the one used in this analysis.

Since fluid flow behaviour impacts on the structure of the pipe walls, the observed stress distribution on the pipe walls would be a result of the flowing fluid impact on the inner walls of the pipes (Fox & Stepnewski, 1974: 258-262, Païdoussis, 1998: 88-104 and Lee *et al.*, 1995: 297-311), and the pipe wall's reaction to the flow effect. However, the maximum stress magnitudes which are shown at the points where flow is constricted are still within the acceptable design stress limit (two thirds of  $8.28 \times 10^2 \text{ N/mm}^2$ ).

The full model of the unwelded pipe experienced a simulated FEA maximum von Mises stress of  $3.18 \text{ N/mm}^2$ , a difference of  $0.03 \text{ N/mm}^2$  less than the calculated hoop stress. The reduced model of the unwelded pipe experienced a simulated FEA maximum von

Mises stress of  $3.17 \text{ N/mm}^2$ , a difference of  $0.04 \text{ N/mm}^2$  less than the calculated hoop stress. The maximum stresses experienced by both unwelded pipe models would not cause any strain on the pipe because they are less than two thirds of  $828 \text{ N/mm}^2$  - the yield strength of titanium alloy (grade 5), considering the pipe's design life and other design conditions.

The stress distribution on the simulated models also showed that the outer walls of the pipe models experienced less stress than the inner walls, where the fluid has a more direct impact (Becht, 2004: 29-35). The 1000 mm model had a simulated maximum von Mises stress of  $3.183 \times 10^2 \text{ N/mm}^2$ , and the 50 mm model had a simulated maximum von Mises stress of  $3.172 \times 10^2 \text{ N/mm}^2$  - a negligible difference of  $0.011 \times 10^2 \text{ N/mm}^2$ . In comparison, the maximum stress values of both models are a little less than the calculated allowable hoop stress value of  $3.21308 \times 10^2 \text{ N/mm}^2$ ; with percentage deviations of 0.94% for the 1000 mm model, and 1.25% for the 50 mm model. The percentage deviations are within the accepted engineering limits of plus or minus two and a half percentage.

#### 4.3.2 The “Circumference Weld” Pipe Models (CW)

On the pipe models welded along the circumference, at a central point equidistant from both ends of the models, maximum stress was shown at the supported points (pipe models' ends) because the flowing fluid impacted turbulently on the walls of the pipe models as a result of flow constriction at the rigidly supported points (Freitas Rachid & Costa Mattos, 1998: 139-160 and Li *et al.*, 2002: 2077-2084). The pipe models were least stressed at a small section adjacent to the inflow supported point and an equivalent small section adjacent to the outflow supported point because the fluid momentarily lost impetus after flow constriction and also before constriction. The lengthy middle section of the 1000 mm pipe model and the middle section of the 50 mm pipe model between the two least stressed sections of both models showed a uniform stress that was more but close to the minimum recorded stress. However, there was less stress shown on the heat affected zone than on the parent material (Figure 4.2a and 4.2b), due probably to the difference in material property and composition (Kalpakjian, 1989: 38-40; Fuji *et al.*,

2001: 25-29. and Askeland, 1996: 428-429). And as previously noted (Beesen, 1999: 3-11), a good welding technique could result in a weld joint with better weld integrity, and would further reduce the stress experienced by the welded product at the weldment and its surrounding heat affected zone.

Even though the stress on the parent material was more than the stress on the surrounding heat affected zone, it was less than the stress shown on the supported points; in much the same way as was the case with the control (unwelded) models. For the 1000 mm model, the heat affected zone showed simulated stress values of between  $0.31 \times 10^2$  N/mm<sup>2</sup> and  $0.60 \times 10^2$  N/mm<sup>2</sup>, and the pipe model's ends showed simulated stress values of  $3.19 \times 10^2$  N/mm<sup>2</sup> and  $0.69 \times 10^2$  N/mm<sup>2</sup>. The 50 mm model showed simulated stress values of between  $0.37 \times 10^2$  N/mm<sup>2</sup> and  $0.69 \times 10^2$  N/mm<sup>2</sup>) at the heat affected zone, while the pipe ends showed simulated stress values of between  $2.89 \times 10^2$  N/mm<sup>2</sup> and  $3.20 \times 10^2$  N/mm<sup>2</sup>. The difference between the simulated maximum stress values of the 1000 mm (full) and 50 mm (reduced) models is negligible -  $0.01 \times 10^2$  N/mm<sup>2</sup>.

From the simulation results, the (simulated) maximum von Mises stress values of  $3.191 \times 10^2$  N/mm<sup>2</sup> (approximately  $3.19 \times 10^2$  N/mm<sup>2</sup>) for the 1000 mm pipe model, and  $3.204 \times 10^2$  N/mm<sup>2</sup> (approximately  $3.20 \times 10^2$  N/mm<sup>2</sup>) for the 50 mm pipe model, are very close to the calculated allowable hoop stress value of  $3.21 \times 10^2$  N/mm<sup>2</sup>. The maximum von Mises stress value of the 1000 mm pipe model gives it a percentage deviation of 0.62% from the calculated hoop stress. The percentage deviation of the 50 mm pipe model from the analytically determined hoop stress value is 0.31%. The two values are also less than two thirds of 828 N/mm<sup>2</sup> - the yield strength of titanium alloy (grade 5), thereby satisfying a primary design criterion.

#### 4.3.3 The “Seam Weld” Pipe Models (SWP)

The simulation results of the pipe models welded along the seam showed that the models experienced minimum stress at a small section adjacent to the inflow and outflow supported points similar to that of the control model, for the same reasons. The flow

constriction at the ends of the pipe models (rigidly supported points) were a result of the pipe models' resistance to gravity and flexural movement in response to the load. The relative turbulence due to the fluid flow constriction impacts on the walls of the pipe models, causing maximum stress at those points along the pipe models (Li *et al.*, 2002: 2077-2084). The lengthy middle section of the pipe models between the two least stressed small sections experienced uniform stress that was shown to be slightly higher than what the least stressed sections experienced. The uniform stress shown on the lengthy section was because the fluid had a consistent steady flow within an unchanged flow boundary (Fox & Stepnewski, 1974: 258-262 and Lee *et al.*, 1995: 297-311).

The simulated maximum von Mises stress value of the 1000 mm pipe model is  $3.18 \times 10^2$  N/mm<sup>2</sup>, while the 50 mm pipe model has a maximum von Mises stress value of  $3.21 \times 10^2$  N/mm<sup>2</sup>; - a difference of  $0.03 \times 10^2$  N/mm<sup>2</sup> between the two seam-welded pipe models. The 1000 mm pipe model showed a stress difference of  $0.00 \times 10^2$  N/mm<sup>2</sup> from the 1000 mm control (unwelded) pipe model, and the 50 mm seam welded model showed a difference of  $0.04 \times 10^2$  N/mm<sup>2</sup> from the 50 mm control (unwelded) pipe model. The percentage deviation of the maximum von Mises stress of the 1000 mm pipe model from the analytically determined hoop stress is 0.94%. And the percentage deviation of the maximum von Mises stress of the 50 mm pipe model from the analytically determined hoop stress is 0.00%. The maximum von Mises stress values shown on the two models are a little less than the calculated allowable hoop stress value of  $3.21 \times 10^2$  N/mm<sup>2</sup>. Though the simulated maximum von Mises stress values of the seam welded pipe models had shown to be pretty close to the calculated hoop stress value, in practice, adjoining pipes in pipeline networks are not connected (welded to one another) along their seams. Rather, they are realistically connected to one another by joints made around their circumference.

#### 4.3.4 Discussion

The finite element analysis results of all the pipe models are in agreement with the analytically determined hoop stress value. Apart from the percentage deviation of the

maximum von Mises stress values of each of the pipe models from the analytically determined hoop stress value, piping design standards were also considered. The industry acceptable stress limit of materials when put under maximum desired load is that they be less than or equal to two thirds of their yield strength ([www.absa.ca](http://www.absa.ca)). The Finite Element Analysis (FEA) results of all three sets of pipe models analysed satisfy this condition too. The six pipe models showed maximum von Mises stress values that are less than two thirds of 828 MPa - the yield strength of titanium alloy (grade 5).

The stress distribution along the three sets of pipe models were shown to be the same regardless of the welding position. All six models experienced uniform low stress in the middle section and comparatively higher stress at the ends. The magnitudes of the maximum stress shown on all six pipe models were very close, with the 50 mm unwelded pipe model showing the lowest ( $3.17 \times 10^2$  N/mm<sup>2</sup>) and the 50 mm seam welded model showing the highest magnitude of  $3.21 \times 10^2$  N/mm<sup>2</sup>.

## Chapter 5 Conclusion

Models of titanium alloy (grade 5) pipes with an Outside diameter of 8.625 inches (219.075 mm), and an inner diameter of 8.500 inches (206.375 mm) were created using Pro/ENGINEER Wildfire 5.0. The pipe models were subjected to Finite Element Analysis using the same software, which employs the Finite Element Method. All the results showing the magnitude of the maximum von Mises stress obtained from the Finite Element Analysis were within industry acceptable stress limits. They satisfy the important condition that the stress limits of materials when put under maximum desired load be less than or equal to two thirds of their yield strength, 828 MPa in the case of Ti6Al4V.

The FEA results of the reduced models were quite close to those of the full models. The difference between the magnitude of the least of the maximum von Mises stress results and that of the highest of the maximum von Mises stress results shown was  $0.04 \times 10^2$  N/mm<sup>2</sup>. The stress distribution shown by the Finite Element Analysis results were consistent for all the Ti6Al4V pipe models. The maximum von Mises stress of all six models were in agreement with the analytically determined hoop stress value of  $3.21 \times 10^2$  N/mm<sup>2</sup>.

The results obtained from this research work indicate that welded titanium alloy (grade 5) pipes can withstand as much stress as unwelded titanium alloy (grade 5) pipes, when used as fluid conduit. The results also show that welded Ti6Al4V would be fit for use as material for pipes in transporting fluid.

## REFERENCES

- (<http://www.absa.ca/IBIndex/IB05-001.pdf>). Last accessed in April, 2009.
- ([http://www.azom.com/Details.asp?ArticleID=1245#\\_Heat\\_Treating\\_Titanium](http://www.azom.com/Details.asp?ArticleID=1245#_Heat_Treating_Titanium)). Last accessed in September, 2008.
- (<http://www.keytometals.com/default.aspx?ID=CheckArticle&NM=136>). Last accessed in September, 2008.
- (<http://www.ptc.com/community/resource-center/proengineer/index.htm>). [Click ‘Help’, click ‘Help center’, click ‘Simulation’, click ‘Pro/ENGINEER Mechanica’, click ‘Search’, type ‘log life’, press ‘enter’, click ‘Fatigue Analysis Overview’].
- ([http://www.timet.com/index\\_new.htm](http://www.timet.com/index_new.htm)). Last accessed in December, 2008.
- (<http://www.twi.co.uk/content/jk24.html>). Last accessed in January , 2009.
- (<http://www.wtia.com.au/pdf/TGN-MS-02%20Titanium.pdf>). Last accessed in January, 2009.
- ([http://www.vogeltool.com/pipe\\_schedules.html](http://www.vogeltool.com/pipe_schedules.html)). Last accessed in September, 2008.
- ADAMS, C.M. 1958. Cooling Rates and Peak Temperature in Friction Welding. *Welding Journal (N.Y)*, 37: 210.
- ASKELAND, D.R. 1996. *The Science and Engineering of Materials*. Chapman & Hall.
- BARKSDALE & JELKS 1968. Titanium. In Hampell, C.A., ed. *The Encyclopaedia of the Chemical Elements*. Reinhold Book Corporation.

BECHT, C. 2005. New Weld Joint Strength Reduction Factor. *Proceedings*. American Society of Mechanical Engineers, New York. 2006.

BLISCHKE, W.R. & MURTHY, D.N.P. 2000. *Reliability: Modelling, Prediction and Optimization*. Wiley & IEEE.

BOYER, R., COLLINGS, E.W. & WELSCH, G. 1994. *Materials Properties Handbook: Titanium Alloys*. ASM International.

BURGESS, N.T. 1989. *Quality Assurance of welded construction*. Taylor and Francis.

CAMPBELL, F.C. 2006. *Manufacturing Technology for Aerospace Structural Materials*. Elsevier.

CARY, H. B. & HELZER, S.C. 2005. *Modern Welding Technology*. Pearson Education.

CHABAK, A. 2010. Tank and Material for Storage of Hydrogen Gas. *United States Pattern, no., US 7,648,567 B2*. 8-9.

CHATURVEDI, M.C., XU, Q. & RICHARDS, N.L. 1997. Electron beam welding of a Ti-45Al-2Nb-2Mn+0.8 vol% TiB<sub>2</sub> XD alloy. *Elsevier/ Material Science and Engineering*, A1: 239-240.

CHATURVEDI, M.C., XU, Q. & RICHARDS, N.L. 1999. The Role of Phase Transformation in Electron-Beam Welding of TiAl-Based Alloys. *Metallurgical and Materials Transaction*, A1: 130-134.

CHEN, Z. & ZHANG, W. 1998. Stability Analysis of Simple Pipe System Conveying Fluid. *Journal of Vibration Engineering*, 11: 38-45.

CLARK, D.S. & VARNEY, W.R. 1965. *Physical Metallurgy for Engineers*. D. Van Nostrand.

DANIELSON, P., WILSON, R. & ALMAN, D. 2003. Microstructure of Titanium Welds. *Struers Journal of Materialography*, 3/2004: 2-7.

DAVID, S.A. 2003. Trends in Welding Research. *Proceedings*. 6th International Conference, Phoenix, Arizona, ASM International, 15-19 April 2002. Ohio: 1022.

DAVID, S.A., DEBROY, T., LIPPOLD, J.C., SMART, H.B. & VITEK, J.M. 2005, Trends in Welding Research, *Proceedings*. 7th International Conference, Georgia, USA, ASM International, 67-81, 85-91.

DE, A., GUPTA, O.P. & DORN, L. 1996. An Experimental Study of Resistance Spot Welding in 1mm Thick Sheet of Low Carbon Steel. *Journal of Engineering Manufacture, Institute of Mechanical Engineers*, B210: 23-26.

DEN HARTOG, M.J. 1961. *Strength of Materials*, Dover Publications.

DONACHIE, M.J. 2000. *Titanium: A Technical Guide*. Ohio: ASM International.

ELMER, J.W. & WONG, J. 2001. Welding Science – A New Look at a Fundamental Technology. *Lawrence Livermore National Laboratory/Science & Technology Review*, 79(4): 1-11.

FOLKHARD, E., RABENSTEINER, G., PERTENEDER, E., SCHABEREITER, H. & TOSCH, J. 1987. *Welding Metallurgy of Stainless Steel*. Springer-Verlag/Wein.

FOX, G.L. & STEPNEWSKI, D.D. 1974. Pressure Wave Transmission in a Fluid contained in a Plastically Deforming Pipe. *Journal of Pressure Vessel Technology*, 96: 258-262.

FREITAS RACHID, F.B. & COSTA MATTOS, H.S. 1994. Model for Structural Failure of Elasto-viscoplastic Pipelines. *Meccanica*, 29: 293-304.

FREITAS RACHID, F.B. & COSTA MATTOS, H.S. 1998. Modelling the Damage Induced by Pressure Transients in Elasto-Plastic Pipes. *Meccanica*, 33: 139-160.

FREITAS RACHID, F.B., SALDANHA DA GAMA, R.M. & COSTA MATTOS, H.S. 1994. Modelling of Hydraulic Transients in Damageable Elasto-viscoplastic Piping Systems. *Journal of Applied Mathematical Modelling*, 18: 207-215.

FREITAS RACHID, F.B., STUCKEMBRUK, S. & COSTA MATTOS, H.S. 1991. Fluid-Structure Interaction in Elastoviscoplastic Piping Systems. *Proceeding. 1st ASME-JSME Fluids Engineering Conference*, 107: 65-73.

FUJI, A., AMEYAMA, K., KOKAWA, H., SATOH, Y. & NORTH, T. H. 2001. Properties of As Welded and Heat Treated Pure Titanium-7075 Al-Zn-Mg Alloy Friction Weld Joints. *Science and Technology of Welding and Joining*, 6(1): 23-30.

GORMAN, D.G., REESE, J.M. & ZHANG, Y.L. 2000. Vibration of a Flexible Pipe Conveying Viscous Pulsating Fluid Flow. *Journal of Sound and Vibration*, 230: 379-392.

HADJ-SADOK, C., PAYEN, T. & DE LANGRE, E. 1997. Nonlinear Vibrations of Loosely Supported Tubes excited by Fluidelastic and Turbulence Forces. *Proceedings. ASME 1997 International Mechanical Engineering Congress and Exposition, Dallas*, 193-199.

HASS, D. 2006. *Titanium – You Can Weld It*. Fabricators and Manufacturers Association, International.

HAWKINS, R.C. 2008. Replacing Corroded and Failed Metallic Pipe with Corrosion Resistant FRP Pipe Design and Installation Requirements and a case History.

*Proceedings.* Corrosion/NACE International, 16-20 March 2008. New Orleans LA: 8516-8523.

HICKS, T. G. 2006. *Handbook of Mechanical Engineering Calculations*. McGraw-Hill.

INOUE, H., OHKITA, S. & NAGATANI, T. 2002. Weld Cracking and Solidification Behaviour of Titanium Alloys, *Welding Journal*, 74(1): 21-27.

JAMES, AULT, PILLERS, VEECK & STEWART. 2005. GTAW of Ti-6Al-4V Castings and Its Effect on Microstructural and Mechanical Properties. *Journal of the Minerals, Metals and Materials Society*, 57(11): 62-65.

JEFFUS, L.F. 1997. Welding: Principles and Application. Cengage Learning.

KALPAKJIAN, S. 1989. *Manufacturing Engineering and Technology*. Addison-Wesley.

KALPAKJIAN, S. & SCHMID, S. R. 2001. *Manufacturing Engineering and Technology*. Prentice Hall.

KENNEDY, J.L. 1993. *Oil and Gas Pipeline Fundamentals*. 2nd ed. Penn well Books.

KUNTJORO, W. 2006. *An Introduction to the Finite Element Method*. McGraw-Hall Higher Education.

KRUGLOV, A.A., ENIKEEV, F.U. & LUTFULLIN, R. Ya. 2001. Superplastic forming of a spherical shell out of a welded envelope. *Material Science and Engineering*, A323 (2002): 416-426.

LEE, U. & KIM, J. 1999. Dynamics of Branched Pipeline Systems Conveying Internal Unsteady Flow. *Journal of Vibration and Acoustics*, 121: 114-122.

- LEE, U., PAK, C.H. & HONG, S.C. 1995. The Dynamics of a Piping System with Internal Unsteady Flow. *Journal of Sound and Vibration*, 180: 297-311.
- LIN, C.W. 1996. Design Guide to Reduce Potential for Vibration caused by Fluid Flow inside Pipes – Review And Survey. *Welding Research Council Bulletin*, 417: 1-28.
- LUTJERING, G. & WILLIAMS, J.C. 2003. *Titanium: Engineering Materials and Processes*. Springer.
- MCALLISTER, E.W. 2005. *Pipeline Rules of Thumb Handbook*, 6th ed. Guly Professional Publishing.
- MICHELIN, A. 2010. Understanding More About Titanium Welding. *Ezine*, 5105093: 210-216.
- MINNICK & WILLIAM, H. 1996. *Gas Tungsten Arc Welding handbook*. Goodheart-Willcox.
- NIORDSON, F.I.N. 1953. Vibrations of a Cylindrical Tube containing Flowing Fluid. *Transactions*. Royal Institute of Technology, (73): 1-28.
- NOBUYUKI, F., YOSHIMASA, F., TERUHIKO, H. & KATSUHIKO, Y. 2002. Inspection of Weld Zone and Joint Performance – Welding of Pure Titanium and Joint Performance (Report 2). *Welding Research Abroad*, 48(4): 56-64.
- O'BRIEN, R.L. 1991. *Welding Handbook*. American Welding Society.
- PAHL, G. & BEITZ, W. 1988. *Engineering Design – A Systematic Approach*. The Design Council/Springer.

PAÏDOUSSIS, M.P. 1998. *Fluid-Structure Interactions, Volume 1: Slender Structures and Axial Flow*. San Diego, CA: Academic Press.

PEDERSEN, J. & HENON, B.K. 2002. Orbital Welding of Titanium Pipe for Troll and Heidrun Offshore Production Platforms. *Stainless Steel World*, 32(1): 50-53.

PETTIGREW, M.J., TAYLOR, C.E., FISHER, N.J., YETSIR, M. & SMITH, B.A. 1998. Flow-induced Vibration: Recent Findings and Open Questions. *Nuclear Engineering and Design*, 185: 249-276.

POLMEAR, I.J. 2006. *Light Alloys – From Traditional Alloys to Non-crystal*. 4th ed. Elsevier.

PORTER, D.A. & EASTERLING, K.E. 1995. *Phase Transformations in Metals and Alloys*. Chapman & Hall.

RADULESCA, A. 2006. Welding Safety and Certification. *Ezine*, 84: 30-37.

RUSSELL, M.J. 2003. *Friction Stir Welding of Titanium Alloys - A Progen Update*. Thomson/The Welding Institute.

SCHULTZ & HELMUT. 1993. *Electron Beam Welding*. Woodhead Publishing/The Welding Institute.

SHARMA, P.C. & AGGARWAL, D.K. 2003. *Machine Design*. Sanjeev Kumar Kataria.

SHEHATA, M.T., ELBOUJDAINI, M & REVIE, R.W. 2008. Initiation of Stress Corrosion Cracking and Hydrogen-Induced Cracking in Oil and Gas Line-Pipe Steels. In Safety, Reliability and Risks associated with Water, Oil and Gas Pipelines. *Chemistry and Material Science/NATO Science for Peace and Security Series C: Environmental Security*, DOI: 10.1007/978-1-4020-6526-2\_7: 115-129.

- SHIGLEY, J.E. 1986. *Mechanical Engineering Design*. McGraw-Hill.
- SHIGLEY, J.E., MISCHKE, C.R. & BUDYNAS, G.R. 2004. *Mechanical Engineering Design*. McGraw-Hill.
- SISTA, J., YANG, Z., ELMER, J. & DEBROY, T. 2000. Three Dimensional Monte Carlo Simulation of Grain Growth During GTA Welding of Titanium. *Acta Materialia*, 48(20): 4813-4825.
- SLUZALEC, A. 1986. Modelling of Titanium Weld Failure. *Computers & Structures/Pergamum*, 28(1): 53-58.
- SMALLMAN, R.E. & NGAN, A.H.W. 2007. *Physical Metallurgy and Advanced Materials*. 7th ed. Elsevier.
- SMITH, L.S., THREADGILL, P. & GITTOES, M. 1999. *Welding Titanium: A Designers and Users Handbook*. TWI & the Titanium Information Group.
- SMITH, W.F. 1981. *Structure and Properties of Engineering Alloys*. McGraw-Hill.
- STOLOFF, N.S. & SIKKA, V.K. 1996. *Physical Metallurgy and Processing of Intermetallic Compounds*. New York: Chapman and Hall.
- STRANG, W.G. & FIX, G.J. 1973. *An Analysis of the Finite Element Method*. Prentice-Hall.
- THREADGILL, P. 2008. Linear Friction Welding. *TWI and the Titanium Lyamats Group*, 61: 335-340.

TIVELLI, M.M. 2004. Innovation in Mature Industries: Recent Impact of the Oil & Gas and Automobile Technological Trends on the Steel Industry. *Massachusetts Institute of Technology*. 10-14.

VAIRIS, A. & FROST, M. 2000. Modelling the linear friction welding of titanium blocks. *Materials Science and Engineering*, A292(1): 8-17.

WEMAN, K. 2003. *Welding processes handbook*. CRC Press.

YANG, Z., ELMER, J.W., WONG, J. & DeBROY, T. 2000. Evolution of Titanium Arc Weldment Macro and Microstructures – Modelling and Real Time Mapping of Phases. *Welding Journal Research Supplement (Miami)*, 79(4): 97-112.

YOUNGDAHL, C.K. & KOT, C.A. 1975. Effect of Plastic Deformation of Piping on Fluid-Transient Propagation. *Nuclear Engineering and Design*, 35: 315-325.

YUNLIAN, Q., JU, D., QUAN, H. & LIYING, Z. 2000. Electron beam welding, Laser beam welding and Gas tungsten arc welding of Titanium sheet. *Material Science and Engineering*, A280(1): 177-181.

**Appendix A****Simulation result Summary for Structural (static) Design  
Study of 1000 mm "unwelded" pipe model**

---

Mechanica Structure Version L-03-40:spg  
Summary for Design Study "full\_unwelded2\_29dec10"  
Wed Dec 29, 2010 11:21:12

---

**Run Settings**

Memory allocation for block solver: 128.0

**Parallel Processing Status**

Parallel task limit for current run: 8

Parallel task limit for current platform: 64

Number of processors detected automatically: 8

Checking the model before creating elements...

These checks take into account the fact that AutoGEM will automatically create elements in volumes with material properties, on surfaces with shell properties, and on curves with beam section properties.

Generate elements automatically.

Checking the model after creating elements...

No errors were found in the model.

Mechanica Structure Model Summary

Principal System of Units: millimeter Newton Second (mmNs)

Length: mm

Force: N

Time: sec

Temperature: C

Model Type: Three Dimensional

Points: 1103

Edges: 5399

Faces: 7490

Springs: 0

Masses: 0

Beams: 0

Shells: 0

Solids: 3194

Elements: 3194

---

## Standard Design Study

Static Analysis "full\_unwelded2\_29dec10":

Convergence Method: Multiple-Pass Adaptive  
Plotting Grid: 10

Convergence Loop Log: (11:21:18)

>> Pass 1 <<

Calculating Element Equations (11:21:18)  
Total Number of Equations: 3057  
Maximum Edge Order: 1  
Solving Equations (11:21:19)  
Post-Processing Solution (11:21:19)  
Calculating Disp and Stress Results (11:21:19)  
Checking Convergence (11:22:03)  
Elements Not Converged: 3194  
Edges Not Converged: 5399  
Local Disp/Energy Index: 100.0%  
Global RMS Stress Index: 100.0%  
Resource Check (11:22:03)  
Elapsed Time (sec): 51.33  
CPU Time (sec): 22.47  
Memory Usage (kb): 294036  
Wrk Dir Dsk Usage (kb): 24576

>> Pass 2 <<

Calculating Element Equations (11:22:03)  
Total Number of Equations: 18750  
Maximum Edge Order: 2  
Solving Equations (11:22:05)  
Post-Processing Solution (11:22:06)  
Calculating Disp and Stress Results (11:22:07)  
Checking Convergence (11:22:44)  
Elements Not Converged: 1305  
Edges Not Converged: 3438  
Local Disp/Energy Index: 100.0%  
Global RMS Stress Index: 28.3%  
Resource Check (11:22:45)  
Elapsed Time (sec): 92.86  
CPU Time (sec): 40.95  
Memory Usage (kb): 317972  
Wrk Dir Dsk Usage (kb): 24576

>> Pass 3 <<

Calculating Element Equations (11:22:45)  
Total Number of Equations: 57960  
Maximum Edge Order: 4  
Solving Equations (11:22:50)  
Post-Processing Solution (11:22:55)  
Calculating Disp and Stress Results (11:22:57)  
Checking Convergence (11:23:31)  
Elements Not Converged: 443  
Edges Not Converged: 877  
Local Disp/Energy Index: 74.1%  
Global RMS Stress Index: 8.4%  
Resource Check (11:23:32)  
Elapsed Time (sec): 139.61  
CPU Time (sec): 77.84  
Memory Usage (kb): 326612  
Wrk Dir Dsk Usage (kb): 199680

>> Pass 4 <<

Calculating Element Equations (11:23:32)  
Total Number of Equations: 75195  
Maximum Edge Order: 4  
Solving Equations (11:23:39)  
Post-Processing Solution (11:23:47)  
Calculating Disp and Stress Results (11:23:49)  
Checking Convergence (11:24:37)  
Elements Not Converged: 98  
Edges Not Converged: 233  
Local Disp/Energy Index: 29.6%  
Global RMS Stress Index: 8.8%  
Resource Check (11:24:37)  
Elapsed Time (sec): 205.56  
CPU Time (sec): 124.58  
Memory Usage (kb): 334932  
Wrk Dir Dsk Usage (kb): 273408

>> Pass 5 <<

Calculating Element Equations (11:24:38)  
Total Number of Equations: 90390  
Maximum Edge Order: 5  
Solving Equations (11:24:44)  
Post-Processing Solution (11:24:53)  
Calculating Disp and Stress Results (11:24:56)  
Checking Convergence (11:25:48)  
Elements Not Converged: 0  
Edges Not Converged: 0

Local Disp/Energy Index: 8.7%  
Global RMS Stress Index: 1.6%

RMS Stress Error Estimates:

Load Set	Stress Error	% of Max Prin Str
SummedLoadSet	4.09e+00	0.7% of 5.49e+02
Resource Check	(11:25:58)	
Elapsed Time (sec):	286.19	
CPU Time (sec):	191.30	
Memory Usage (kb):	342996	
Wrk Dir Dsk Usage (kb):	355328	

The analysis converged to within 10% on edge displacement, element strain energy, and global RMS stress.

Total Mass of Model: 1.889806e-02

Total Cost of Model: 0.000000e+00

Mass Moments of Inertia about WCS Origin:

Ixx: 2.13984e+02  
Ixy: -5.09331e-07 Iyy: 6.40634e+03  
Ixz: -2.05874e-08 Iyz: -3.83867e-08 Izz: 6.40634e+03

Principal MMOI and Principal Axes Relative to WCS Origin:

Max Prin	Mid Prin	Min Prin
6.40634e+03	6.40634e+03	2.13984e+02
WCS X: 0.00000e+00	0.00000e+00	1.00000e+00
WCS Y: 1.00000e+00	0.00000e+00	0.00000e+00
WCS Z: 0.00000e+00	1.00000e+00	0.00000e+00

Center of Mass Location Relative to WCS Origin:  
( 5.00000e+02, 3.43668e-09, -3.72543e-10)

Mass Moments of Inertia about the Center of Mass:

Ixx: 2.13984e+02  
Ixy: -4.76857e-07 Iyy: 1.68183e+03  
Ixz: -2.41076e-08 Iyz: -3.83867e-08 Izz: 1.68183e+03

Principal MMOI and Principal Axes Relative to COM:

Max Prin	Mid Prin	Min Prin
1.68183e+03	1.68183e+03	2.13984e+02

WCS X:	-2.23320e-10	-2.36512e-10	1.00000e+00
WCS Y:	7.22374e-01	6.91503e-01	3.24869e-10
WCS Z:	-6.91503e-01	7.22374e-01	1.64238e-11

Constraint Set: constraint\_full\_unwelded2: FULL\_UNWELDED2

Load Set: SummedLoadSet

gravity_full_unwelded2:	FULL_UNWELDED2
flowrate_full_unwelded2:	FULL_UNWELDED2
pressure_full_unwelded2:	FULL_UNWELDED2

Resultant Load on Model:

in global X direction:	7.117150e+05
in global Y direction:	-1.853890e+02
in global Z direction:	1.230869e-06

Measures:

Name	Value	Convergence
max_beam_bending:	0.000000e+00	0.0%
max_beam_tensile:	0.000000e+00	0.0%
max_beam_torsion:	0.000000e+00	0.0%
max_beam_total:	0.000000e+00	0.0%
max_disp_mag:	2.324932e-01	0.1%
max_disp_x:	1.774877e-01	0.0%
max_disp_y:	-1.783033e-01	0.4%
max_disp_z:	-1.779868e-01	100.0%
max_prin_mag:	5.490336e+02	5.4%
max_rot_mag:	0.000000e+00	0.0%
max_rot_x:	0.000000e+00	0.0%
max_rot_y:	0.000000e+00	0.0%
max_rot_z:	0.000000e+00	0.0%
max_stress_prin:	5.490336e+02	5.4%
max_stress_vm:	3.183438e+02	4.6%
max_stress_xx:	5.000278e+02	5.3%
max_stress_xy:	-1.122798e+02	14.1%
max_stress_xz:	1.129889e+02	5.6%
max_stress_yy:	2.609848e+02	3.4%
max_stress_yz:	-1.019527e+02	6.5%
max_stress_zz:	2.607986e+02	1.4%

min\_stress\_prin: -4.581956e+02 2.9%  
strain\_energy: 5.541451e+05 0.1%

Analysis "full\_unwelded2\_29dec10" Completed (11:25:59)

---

#### Memory and Disk Usage:

Machine Type: Windows NT/x86  
RAM Allocation for Solver (megabytes): 128.0

Total Elapsed Time (seconds): 287.21  
Total CPU Time (seconds): 191.90  
Maximum Memory Usage (kilobytes): 342996  
Working Directory Disk Usage (kilobytes): 355328

Results Directory Size (kilobytes):  
238433 .\full\_unwelded2\_29dec10

Maximum Data Base Working File Sizes (kilobytes):  
238592 .\full\_unwelded2\_29dec10.tmp\kblk1.bas  
99328 .\full\_unwelded2\_29dec10.tmp\kel1.bas  
17408 .\full\_unwelded2\_29dec10.tmp\oel1.bas

---

Run Completed  
Wed Dec 29, 2010 11:25:59

---

**Appendix B****Simulation result Log for Structural (fatigue) Design Study of  
1000 mm "circumference weld" pipe model**

---

Mechanica Structure Version L-01-41:spg  
Log for Design Study "MWP\_FAT\_4AM\_20AUG"  
Wed Aug 20, 2008 03:53:38

---

Begin Creating Database for Design Study

Wed Aug 20, 2008 03:53:38

Elapsed Time (sec): 0.21  
CPU Time (sec): 0.13  
Memory Usage (kb): 26351  
Work Dir Disk Usage (kb): 0

Step Elapsed Time (sec): 0.00  
Step CPU Time (sec): 0.00

Begin Integrated Mode Error Checking

Wed Aug 20, 2008 03:53:38

Elapsed Time (sec): 0.22  
CPU Time (sec): 0.13  
Memory Usage (kb): 26351  
Work Dir Disk Usage (kb): 0

Checking the model before creating elements...

These checks take into account the fact that AutoGEM will automatically create elements in volumes with material properties, on surfaces with shell properties, and on curves with beam section properties.

Step Elapsed Time (sec): 0.08  
Step CPU Time (sec): 0.03

Begin Generating Elements

Wed Aug 20, 2008 03:53:38

Elapsed Time (sec): 0.30  
CPU Time (sec): 0.16  
Memory Usage (kb): 26372  
Work Dir Disk Usage (kb): 0

Copying elements from an existing study model ...

Successfully copied elements from an existing study model.

A complete set of elements already exists.

OK

Step Elapsed Time (sec): 9.31  
Step CPU Time (sec): 9.22

Begin Integrated Mode Error Checking  
Wed Aug 20, 2008 03:53:47

Elapsed Time (sec): 9.61  
CPU Time (sec): 9.37  
Memory Usage (kb): 76084  
Work Dir Disk Usage (kb): 0

Checking the model after creating elements...

No errors were found in the model.

Step Elapsed Time (sec): 1.95  
Step CPU Time (sec): 1.86

Begin Engine Bookkeeping

Wed Aug 20, 2008 03:53:49

Elapsed Time (sec): 11.56  
CPU Time (sec): 11.23  
Memory Usage (kb): 76084  
Work Dir Disk Usage (kb): 0

Step Elapsed Time (sec): 3.99  
Step CPU Time (sec): 3.55

Begin Analysis: "MWP\_FAT\_4AM\_20AUG"

Wed Aug 20, 2008 03:53:53

Elapsed Time (sec): 15.55  
CPU Time (sec): 14.78  
Memory Usage (kb): 132728  
Work Dir Disk Usage (kb): 0

Step Elapsed Time (sec): 9.68  
Step CPU Time (sec): 5.25

Begin Fatigue Life Calculation

Wed Aug 20, 2008 03:54:03

Elapsed Time (sec): 25.23  
CPU Time (sec): 20.03  
Memory Usage (kb): 193840

Work Dir Disk Usage (kb): 0

Step Elapsed Time (sec): 14589.10  
Step CPU Time (sec): 14585.73

Completed Analysis: MWP\_FAT\_4AM\_20AUG  
Wed Aug 20, 2008 07:57:12

Elapsed Time (sec): 14614.34  
CPU Time (sec): 14605.77  
Memory Usage (kb): 205506  
Work Dir Disk Usage (kb): 0

**Appendix C****Simulation result Summary for Structural (static) Design  
Study of 1000 mm "seam weld" pipe model**

---

Mechanica Structure Version L-03-40:spg  
Summary for Design Study "full\_seam\_welded\_2am26dec10"  
Wed Dec 29, 2010 16:58:05

---

**Run Settings**

Memory allocation for block solver: 128.0

**Parallel Processing Status**

Parallel task limit for current run: 8

Parallel task limit for current platform: 64

Number of processors detected automatically: 8

Checking the model before creating elements...

These checks take into account the fact that AutoGEM will automatically create elements in volumes with material properties, on surfaces with shell properties, and on curves with beam section properties.

Generate elements automatically.

Checking the model after creating elements...

No errors were found in the model.

**Mechanica Structure Model Summary**

Principal System of Units: millimeter Newton Second (mmNs)

Length: mm

Force: N

Time: sec

Temperature: C

Model Type: Three Dimensional

Points: 1043

Edges: 5106

Faces: 7087

Springs: 0

Masses: 0

Beams: 0

Shells: 0

Solids: 3024

Elements: 3024

---

## Standard Design Study

Static Analysis "full\_seam\_welded\_2am26dec10":

Convergence Method: Multiple-Pass Adaptive  
Plotting Grid: 10

Convergence Loop Log: (16:58:10)

>> Pass 1 <<

Calculating Element Equations (16:58:10)  
Total Number of Equations: 2883  
Maximum Edge Order: 1  
Solving Equations (16:58:11)  
Post-Processing Solution (16:58:11)  
Calculating Disp and Stress Results (16:58:12)  
Checking Convergence (16:58:53)  
Elements Not Converged: 3024  
Edges Not Converged: 5106  
Local Disp/Energy Index: 100.0%  
Global RMS Stress Index: 100.0%  
Resource Check (16:58:54)  
Elapsed Time (sec): 48.97  
CPU Time (sec): 25.97  
Memory Usage (kb): 290776  
Wrk Dir Dsk Usage (kb): 22528

>> Pass 2 <<

Calculating Element Equations (16:58:54)  
Total Number of Equations: 17709  
Maximum Edge Order: 2  
Solving Equations (16:58:55)  
Post-Processing Solution (16:58:56)  
Calculating Disp and Stress Results (16:58:57)  
Checking Convergence (16:59:33)  
Elements Not Converged: 1373  
Edges Not Converged: 3469  
Local Disp/Energy Index: 96.8%  
Global RMS Stress Index: 30.1%  
Resource Check (16:59:34)  
Elapsed Time (sec): 89.11  
CPU Time (sec): 49.41  
Memory Usage (kb): 313560  
Wrk Dir Dsk Usage (kb): 22528

>> Pass 3 <<

Calculating Element Equations (16:59:34)  
Total Number of Equations: 56046  
Maximum Edge Order: 4  
Solving Equations (16:59:40)  
Post-Processing Solution (16:59:46)  
Calculating Disp and Stress Results (16:59:48)  
Checking Convergence (17:00:24)  
Elements Not Converged: 511  
Edges Not Converged: 991  
Local Disp/Energy Index: 68.7%  
Global RMS Stress Index: 9.1%  
Resource Check (17:00:25)  
Elapsed Time (sec): 140.18  
CPU Time (sec): 94.70  
Memory Usage (kb): 321880  
Wrk Dir Dsk Usage (kb): 189440

>> Pass 4 <<

Calculating Element Equations (17:00:25)  
Total Number of Equations: 74112  
Maximum Edge Order: 5  
Solving Equations (17:00:31)  
Post-Processing Solution (17:00:39)  
Calculating Disp and Stress Results (17:00:41)  
Checking Convergence (17:01:38)  
Elements Not Converged: 133  
Edges Not Converged: 346  
Local Disp/Energy Index: 29.2%  
Global RMS Stress Index: 9.9%  
Resource Check (17:01:38)  
Elapsed Time (sec): 213.89  
CPU Time (sec): 146.61  
Memory Usage (kb): 330648  
Wrk Dir Dsk Usage (kb): 270336

>> Pass 5 <<

Calculating Element Equations (17:01:39)  
Total Number of Equations: 89511  
Maximum Edge Order: 5  
Solving Equations (17:01:45)  
Post-Processing Solution (17:01:54)  
Calculating Disp and Stress Results (17:01:57)  
Checking Convergence (17:02:44)  
Elements Not Converged: 1  
Edges Not Converged: 24  
Local Disp/Energy Index: 12.3%

Global RMS Stress Index: 1.9%  
Resource Check (17:02:45)  
Elapsed Time (sec): 279.98  
CPU Time (sec): 210.01  
Memory Usage (kb): 337112  
Wrk Dir Dsk Usage (kb): 352256

>> Pass 6 <<

Calculating Element Equations (17:02:45)  
Total Number of Equations: 103290  
Maximum Edge Order: 6  
Solving Equations (17:02:53)  
Post-Processing Solution (17:03:05)  
Calculating Disp and Stress Results (17:03:08)  
Checking Convergence (17:04:03)  
Elements Not Converged: 0  
Edges Not Converged: 0  
Local Disp/Energy Index: 2.7%  
Global RMS Stress Index: 1.1%

RMS Stress Error Estimates:

Load Set	Stress Error	% of Max Prin Str
SummedLoadSet	2.88e+00	0.5% of 5.34e+02

Resource Check (17:04:33)  
Elapsed Time (sec): 388.20  
CPU Time (sec): 311.76  
Memory Usage (kb): 340056  
Wrk Dir Dsk Usage (kb): 446464

The analysis converged to within 10% on edge displacement, element strain energy, and global RMS stress.

Total Mass of Model: 1.889652e-02

Total Cost of Model: 0.000000e+00

Mass Moments of Inertia about WCS Origin:

Ixx: 2.13966e+02  
Ixy: 4.89714e-07 Iyy: 6.40582e+03  
Ixz: -8.19801e-02 Iyz: 1.18975e-07 Izz: 6.40583e+03  
Principal MMOI and Principal Axes Relative to WCS Origin:

Max Prin	Mid Prin	Min Prin
6.40583e+03	6.40582e+03	2.13966e+02

WCS X: -1.32400e-05	0.00000e+00	1.00000e+00
WCS Y: 0.00000e+00	1.00000e+00	0.00000e+00
WCS Z: 1.00000e+00	0.00000e+00	1.32400e-05

Center of Mass Location Relative to WCS Origin:  
( 5.00000e+02, -4.34977e-08, 8.67678e-03)

Mass Moments of Inertia about the Center of Mass:

Ixx: 2.13966e+02		
Ixy: 7.87363e-08	Iyy: 1.68168e+03	
Ixz: 4.02803e-07	Iyz: 1.18968e-07	Izz: 1.68170e+03

Principal MMOI and Principal Axes Relative to COM:

Max Prin	Mid Prin	Min Prin
1.68170e+03	1.68168e+03	2.13966e+02

WCS X: 2.74439e-10	5.36435e-11	1.00000e+00
WCS Y: 6.79090e-06	1.00000e+00	-5.36454e-11
WCS Z: 1.00000e+00	-6.79090e-06	-2.74438e-10

Constraint Set: constraint\_full\_seam\_welded: FULL\_SEAM\_WELDED

Load Set: SummedLoadSet

gravity_full_seam_welded: FULL_SEAM_WELDED		
flow_full_seam_welded: FULL_SEAM_WELDED		
pressure_full_seam_welded: FULL_SEAM_WELDED		

Resultant Load on Model:

in global X direction: 8.006800e+01		
in global Y direction: -1.853736e+02		
in global Z direction: -8.977477e-07		

Measures:

Name	Value	Convergence
max_beam_bending:	0.000000e+00	0.0%
max_beam_tensile:	0.000000e+00	0.0%
max_beam_torsion:	0.000000e+00	0.0%
max_beam_total:	0.000000e+00	0.0%

```
max_disp_mag: 1.583147e-01 0.1%
max_disp_x: 2.079850e-02 0.4%
max_disp_y: 1.555445e-01 100.0%
max_disp_z: -1.580808e-01 0.1%
max_prin_mag: 5.337622e+02 5.5%
max_rot_mag: 0.000000e+00 0.0%
max_rot_x: 0.000000e+00 0.0%
max_rot_y: 0.000000e+00 0.0%
max_rot_z: 0.000000e+00 0.0%
max_stress_prin: 5.337622e+02 5.5%
max_stress_vm: 3.184114e+02 8.4%
max_stress_xx: 4.851895e+02 5.1%
max_stress_xy: -1.154734e+02 12.0%
max_stress_xz: -1.277928e+02 17.3%
max_stress_yy: 2.467465e+02 3.2%
max_stress_yz: -1.003217e+02 0.2%
max_stress_zz: 2.436785e+02 4.2%
min_stress_prin: -2.947144e+02 3.7%
strain_energy: 5.129151e+05 0.0%
```

Analysis "full\_seam\_welded\_2am26dec10" Completed (17:04:33)

---

#### Memory and Disk Usage:

Machine Type: Windows NT/x86  
RAM Allocation for Solver (megabytes): 128.0

Total Elapsed Time (seconds): 389.05  
Total CPU Time (seconds): 312.37  
Maximum Memory Usage (kilobytes): 340056  
Working Directory Disk Usage (kilobytes): 446464

Results Directory Size (kilobytes):  
228251 \full\_seam\_welded\_2am26dec10

Maximum Data Base Working File Sizes (kilobytes):  
295936 \full\_seam\_welded\_2am26dec10.tmp\blk1.bas  
130048 \full\_seam\_welded\_2am26dec10.tmp\el1.bas  
20480 \full\_seam\_welded\_2am26dec10.tmp\el1.bas

---

Run Completed  
Wed Dec 29, 2010 17:04:34

---

**Appendix D****Simulation result Log for Structural (fatigue) Design Study of  
50 mm "unwelded" pipe model**

---

Mechanica Structure Version L-01-41:spg  
Log for Design Study "UNWELDED\_R50\_FAT\_1AM\_18SEP"  
Thu Sep 18, 2008 01:34:41

---

Begin Creating Database for Design Study

Thu Sep 18, 2008 01:34:41

Elapsed Time (sec): 0.17  
CPU Time (sec): 0.12  
Memory Usage (kb): 26228  
Work Dir Disk Usage (kb): 0

Step Elapsed Time (sec): 0.00  
Step CPU Time (sec): 0.02

Begin Integrated Mode Error Checking

Thu Sep 18, 2008 01:34:41

Elapsed Time (sec): 0.17  
CPU Time (sec): 0.14  
Memory Usage (kb): 26228  
Work Dir Disk Usage (kb): 0

Checking the model before creating elements...

These checks take into account the fact that AutoGEM will automatically create elements in volumes with material properties, on surfaces with shell properties, and on curves with beam section properties.

Step Elapsed Time (sec): 0.02  
Step CPU Time (sec): 0.02

Begin Generating Elements

Thu Sep 18, 2008 01:34:41

Elapsed Time (sec): 0.19  
CPU Time (sec): 0.16  
Memory Usage (kb): 26228  
Work Dir Disk Usage (kb): 0

Copying elements from an existing study model ...

Successfully copied elements from an existing study model.

A complete set of elements already exists.

OK

Step Elapsed Time (sec): 0.25  
Step CPU Time (sec): 0.25

Begin Integrated Mode Error Checking

Thu Sep 18, 2008 01:34:42

Elapsed Time (sec): 0.44  
CPU Time (sec): 0.41  
Memory Usage (kb): 31844  
Work Dir Disk Usage (kb): 0

Checking the model after creating elements...

No errors were found in the model.

Step Elapsed Time (sec): 0.08  
Step CPU Time (sec): 0.08

Begin Engine Bookkeeping

Thu Sep 18, 2008 01:34:42

Elapsed Time (sec): 0.53  
CPU Time (sec): 0.48  
Memory Usage (kb): 31844  
Work Dir Disk Usage (kb): 0

Step Elapsed Time (sec): 0.16  
Step CPU Time (sec): 0.17

Begin Analysis: "UNWELDED\_R50\_FAT\_1AM\_18SEP"

Thu Sep 18, 2008 01:34:42

Elapsed Time (sec): 0.69  
CPU Time (sec): 0.66  
Memory Usage (kb): 43888  
Work Dir Disk Usage (kb): 0

Step Elapsed Time (sec): 0.13  
Step CPU Time (sec): 0.11

Begin Fatigue Life Calculation

Thu Sep 18, 2008 01:34:42

Elapsed Time (sec): 0.82  
CPU Time (sec): 0.76  
Memory Usage (kb): 47196

Work Dir Disk Usage (kb): 0

Step Elapsed Time (sec): 544.00  
Step CPU Time (sec): 543.81

Completed Analysis: UNWELDED\_R50\_FAT\_1AM\_18SEP

Thu Sep 18, 2008 01:43:46

Elapsed Time (sec): 544.82  
CPU Time (sec): 544.58  
Memory Usage (kb): 47216  
Work Dir Disk Usage (kb): 0